PROCESSING AND MATERIAL CHARACTERIZATION OF CONTINUOUS BASALT
FIBER REINFORCED CERAMIC MATRIX COMPOSITES USING POLYMER DERIVED
CERAMICS

By

SARAH BETH COX
B.S. Georgia Institute of Technology, 2004

A thesis submitted in partial fulfillment of the requirements
for the degree of Masters of Science
in the Department of Materials Science and Engineering
in the College of Engineering and Computer Science
at the University of Central Florida
Orlando, Florida

Summer Term
2014

Major Professor: Jihua Gou

ABSTRACT

The need for high performance vehicles in the aerospace industry requires materials which can withstand high loads and high temperatures. New developments in launch pads and infrastructure must also be made to handle this intense environment with lightweight, reusable, structural materials. By using more functional materials, better performance can be seen in the launch environment, and launch vehicle designs which have not been previously used can be considered. The development of high temperature structural composite materials has been very limited due to the high cost of the materials and the processing needed. Polymer matrix composites can be used for temperatures up to 260°C. Ceramics can take much higher temperatures, but they are difficult to produce and form in bulk volumes. Polymer Derived Ceramics (PDCs) begin as a polymer matrix, allowing a shape to be formed and cured and then to be pyrolized in order to obtain a ceramic with the associated thermal and mechanical properties. The use of basalt in structural and high temperature applications has been under development for over 50 years, yet there has been little published research on the incorporation of basalt fibers as a reinforcement in the composites. In this study, continuous basalt fiber reinforced PDCs have been fabricated and tested for the applicability of this composite system as a high temperature structural composite material. The oxyacetylene torch testing and three point bend testing have been performed on test panels and the test results are presented.

To my wonderful family

Christopher, Madison, Everett

I couldn't have done this without you.

To Dan Koporec

Thank you for always believing

I love you and miss you

ACKNOWLEDGMENTS

TABLE OF CONTENTS

LIST OF FIGURES

LIST OF TABLES

CHAPTER ONE: BACKGROUND

Advanced composite material systems is a growing field in materials engineering. In the aerospace industry, as the need for high performance vehicles grows, the need for materials which can meet these high performance levels becomes even more important. Materials must withstand high loads and high temperatures while remaining lightweight. Along with vehicle development, launch pads and infrastructure must also progress in order to withstand the intense environment from larger launch vehicles as well as launching from remote sites, both on and off Earth. By using more functional materials, better performance can be obtained, and designs which were previously unattainable can now be considered.

Current Launch Pad Configurations

The performance requirements of a launch pad environment is dependent on a variety of factors, including the physical environment and surroundings, the specific configuration of the vehicle (for example, the type of propellants used and the thrust required), and the design of the launch pad structure. Most importantly, designs must take into consideration the thermal effects (both maximum temperature and heat load), the pressure on the surface due to the thrust of the exhaust, and the vibroacoustical loading due to the recirculation of the exhaust. Characterizing the launch pad environment is a complex task which requires a combination of analytical models and test data. Although modeling of the launch environment is a growing field due to the sophistication of the computer models, assumptions must still be made and conservatism applied. Testing of a launch environment is limited due to the extreme conditions during a launch and the availability of sensors that can withstand the environment and record accurate data.

Commercial Launch Vehicles

Commercial launch vehicles in the United States are comprised of a handful of unmanned rockets which are launched from Cape Canaveral Air Force Station in Florida, Wallops Flight Facility in Virginia, and Vandenberg Air Force Base in California. There is very little information published on these launch pad environments, structural designs, and the materials used for these locations. Consequently, assessment of the current standards and the requirements presents a challenge.

NASA Launch Vehicles for Manned Missions

The Space Shuttle was a more complex system than the expendable launch vehicles. The Space Shuttle could carry up to 55,000 lbs to low earth orbit, and between the three main engines and the two solid rocket boosters, over 6.5 million lbs of thrust were generated. Due to the size of the Space Shuttle Program and its greater awareness in the public consciousness, more interest and resources were available to collect data on the launch environment. The launch pad configuration is shown in Figure 1. The two solid rocket motors used a flame trench on one side of the launch pad, and the three main engines on the orbiter used a separate flame deflector on the opposite side. Due to the amount of thrust required for a shuttle launch, a much stronger and more heat resistant launch pad structure was required than what is used currently for unmanned launch vehicles. The Shuttle's launch pads at Launch Complex 39 use a combination of refractory concrete and a water suppression system. The main function of a water suppression system is to dampen the acoustic loading and prevent it from rebounding and affecting the vehicle.
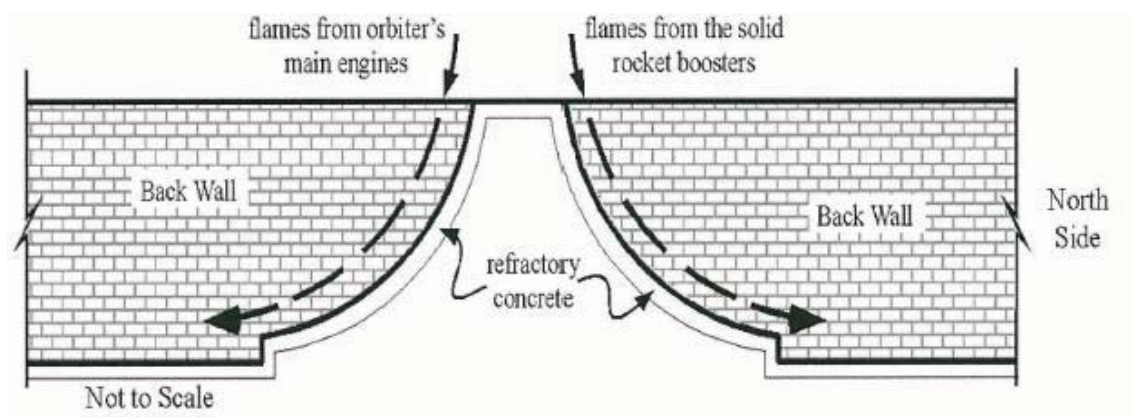
Figure 1: Schematic of Space Shuttle Flame Trench (Credit: (Calle et al., 2010))

After every launch, the pad was inspected for signs of damage. On May 31, 2008, after what seemed to be a perfect launch for STS-124, the recovery team headed out to the pad to find that thousands of the refractory concrete bricks had liberated from the flame trenches. Bricks were found as far as 1800 feet away and traveled as fast as 680 miles per hour. There was significant damage to the flame trench structure due to heating exposure where the bricks had liberated, and the overall cost of repair was around $2.5 million. (System failure case studies: Hit the bricks.2010) This event provided an opportunity for several studies to be performed on the true launch environment as well as testing of the materials that were qualified for use. Launch Pad 39A was instrumented in the solid rocket booster flame trench to take measurements during the last three launches of the Space Shuttle Program. Although there was some sensor failure during each launch, between the three launches, there was enough accurate data recorded during the four second plume impingement to provide an assessment of the true launch environment. The pressure was recorded using Kulite® and Stellar® pressure tranducers. This testing found that the pressure near the top of the flame trench was as high as 0.5 MPa (70 psig), over twice

what is called out in GP-1059, which was the Space Shuttle specification for the thermal and pressure environment at the launch pad. The ignition overpressure at Mission Elapsed Time (MET) + 0.3 seconds spiked to 1.1 MPa (160 psig) in the middle of the flame trench. Another finding was that at the bottom of the flame trench, negative pressure was recorded, indicating a partial vacuum condition, until around MET + 3 seconds, after which point the vehicle is traversing across the pad and the plume is directly impinging at this location. (von Eckroth et al., 2012)

Thermal measurements were recorded by a Medtherm® calorimeter and Nanmac® erodible thermocouples. Additionally, a Tungsten Piston calorimeter was developed at Kennedy Space Center which could withstand the plume and be used in comparison with the other sensors. The temperature sensors located at the top of the flame trench failed during all three launches. Before data cutoff, the highest temperature value recorded at MET + 3.3 was 1180°C (2160°F), which is only about half of what is predicted in GP-1059. The authors of this study suggest this incongruity results from a boundary layer formed across the flame trench surface, insulating it from the higher heat. They suggest that "factors contributing to the formation of the boundary layer include the sound suppression system water, the supersonic plume speed, and the undulations in the [flame deflector] surface." The average maximum heat rate from all the recorded data is 908 W/cm^2 (800 BTU/ft^2-sec), which is about ¼ of the value in GP-1059. Overall heating for the 4 second event is around 2.5 KJ/cm^2 (2200 BTU/ft^2), while GP-1059 gives this value as 9 KJ/cm^2 (8000 BTU/ft^2). The authors suggest that this discrepancy is due to the short duration spikes up to 3500 BTU/ft^2-sec, which occur throughout the launch as the alumina particles, or slag, are ejected from the plume and contact the sensor. The original authors

of GP-1059 would not have been able to measure the short duration of these events due to the instrumentation available at that time; this caused the requirement to be overly conservative. The heat rate for the gaseous portion of the plume was measured to be around 350 BTU/ft^2-sec. (von Eckroth et al., 2012)

The vibrational loads were measured with PCB® accelerometers. A sensor was also placed in a location that did not see direct impingement from the plume, in order to measure the acoustic loading. The peak recorded is around 15 psig, with a sustained value of 10 psig; the sustainment is only for 2 seconds. (von Eckroth et al., 2012)

Current Materials in Use

Most unmanned launch structures are comprised of carbon steel structures which use a water deluge system for both heat and sound suppression. Steel structures are commonly used because of their high temperature capabilities. Again, there is little published information on the performance of these structures.

The Shuttle's launch pads at Launch Complex 39 used a refractory concrete, designed to specification KSC-SPEC-P-0012, in order to protect the areas which see the highest heat and pressure loading during a launch. The concrete requirements pertinent to this study are that it shall have a compressive strength of 31 MPa (4500 psi), and when exposed to a heat flux up to 3750 W/cm^2 (3300 BTU/ft^2-sec) for 10 seconds, it "shall not crack, spall, or erode more than 1/8 inch." The material must also be able to handle the natural environment of the launch pad, such as humidity and sea salt exposure, without degradation of properties. (*Refractory concrete, specification for* 1979)

A study completed at Kennedy Space Center in 2010 compared Fondue Fyre, which is the only qualified refractory material for use at the Launch Complex 39 pads, with two other materials: Ultra-Tek FS Gun Mix and Kruzite GR Plus. Two Fondue Fyre samples were tested; one prepared per the manufacturer, and the other one prepared at the pad as would be done for a repair. All of the specimens were made using the gunite method. After manufacture, the specimens were subjected to a variety of testing, including bending, thermal shock, and compression after environmental conditioning. Modulus of rupture was determined with 3 point bending per ASTM C133: Standard Test Methods for Cold Crushing Strength and Modulus of Rupture of Refractories. Compression strength was tested per ASTM C133 on a control sample as well as after three different exposures: environmental exposure at the Corrosion Technology Laboratory Beachside Atmospheric Exposure Facility, located at Kennedy Space Center; submerged in water for 1 month, to simulate the sound suppression system deluge during launch; and submerged in .1M hydrochloric acid for 10 days, to simulate the solid rocket booster plume. Thermal shock testing was conducted similarly to ASTM C1171. The specimens were subjected to 3 thermal cycles which consisted of 15 minutes at 1100°C followed by 10 minutes at room temperature.

Table 1: Compression Values for Materials Tested (values based on Figure 7 in (Calle et al., 2010))

Compressive Strength (MPa)				
	Nominal	Environmental Exposure	Water Submersion	HCl Submersion
KSC-SPEC-P-0012	31			
Fondue Fyre		18	11	22
Fondue Fyre Pad	26	29	15	27
Ultra-Tek	30	32	22	27
Kruzite	45	51	39	43

As it can be seen in Table 1, this study found that the other materials tested had better compressive strength than the approved Fondue Fyre, which did not meet compressive strength requirement for any of the conditions. The modulus of rupture data is given in Table 2. Although there is no requirement in KSC-SPEC-P-0012, there is a similar trend as the compression data. (Calle et al., 2010)

Table 2. Modulus of Rupture Values for Materials Tested (values based on Figure 8 in (Calle et al., 2010))

Modulus of Rupture (MPa)		
	Ambient	Thermal Shock
KSC-SPEC-P-0012	None Given	
Fondue Fyre	6	2
Fondue Fyre Pad	4	1
Ultra-Tek	6	5
Kruzite	10	5

Based on the most recent launch pad environment data, and the measured performance of existing materials, additional studies will be required to support future used of the existing launch pads.

Future Launch Pad Requirements

Kennedy Space Center is investigating the development of a portable and deployable launch pad system which will have the capability to be transported and assembled at any location. As future mission plans include hardware architectures using much smaller vehicles than the heritage Saturn V and Space Shuttle rockets, this type of launch system is becoming necessary for a variety of applications. For example, Morpheus, shown in Figure 2, is a vertical takeoff/ vertical landing systems designed to carry an 1100-lb payload from the lunar surface. A test vehicle has been built at Johnson Space Center and is now being flight-tested at Kennedy Space Center. The propellant system uses liquid oxygen and methane and the exhaust nozzle is located directly underneath the spacecraft. For the testing of this spacecraft, a portable launch pad must be built that will require minimal refurbishment and can easily be relocated between tests. (Project morpheus.)

Figure 2 Morpheus Lander (credit: www.nasa.gov)

Another portable launch pad application is for launch vehicles specifically developed for smaller payloads. These small payloads, or nanosatellites, are developed by industry, government, and academia to collect data and perform experiments in microgravity. Currently, these types of payloads are secondary to a larger payload on a launch vehicle. This has the benefit of reducing the launch cost, but it is then restricted to the schedule and the orbit of the primary payload. As the demand for this service continues to grow, more efficient and effective deployment would be provided by launch systems designed specifically for these payloads. SWORDS (Soldier-Warfighter Operationally Responsive Deployer for Space), shown in Figure 3, is a collaboration between the Office of the Secretary of Defense, U.S. Army Space and Missile Defense Command/Army Forces Strategic Command, and NASA to develop a launch system which will deliver nanosatellites to orbit as a primary payload at a reduced cost. SWORDS will have the capability to launch a 55-lb payload into orbit. It uses liquid oxygen and methane for the propellant. The launch system must have the ability to launch quickly from a variety of locations, depending on the orbit requirements of the payload. These locations will have minimal infrastructure, requiring a portable, deployable launch pad. (SWORDS: Soldier-warfighter operationally responsive deployer for space.)
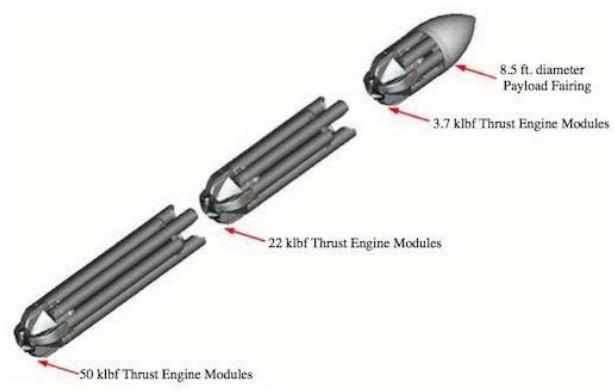
Figure 3 SWORDS Launcher (http://www.smdc.army.mil/FactSheets/SWORDS.pdf)

These are just two examples of the need for a deployable, lightweight launch structure. Carbon steel and refractory concrete are less than ideal materials for this type of structure due to their weight and the necessary infrastructure. Materials developed for launch pad structures must be able to handle the harsh environment during launch and be reusable with minimal refurbishment between launches. This requires the materials to be able to survive in the launch environment with minimal degradation. In addition, the desired portability of the launch pad requires the structure to be lightweight; Ease of transportation becomes an important consideration, as does assembly without the need for a large crane or other heavy lift equipment. Development of a launch pad that is reusable and lightweight will reduce the costs of refurbishment and transportation.

<u>A New Launch Pad Structure Material</u>

The standard materials that have been used for the Space Shuttle pads as well as the expendable launch vehicles have been adequate, but with the need for smaller deployable pads, other materials need to be explored. Fiber reinforced composites have become more prevalent as structural materials because of their strength to weight ratio. The combination of fibers and matrix can be tailored to specifically meet unique requirements. This would be ideal for a lightweight, high temperature application. Ceramic matrix composites maintain their properties at high temperatures, and the continuous fiber reinforcement provides increased strength in an otherwise brittle material. In this study, a ceramic matrix composite is fabricated and tested for high temperature and mechanical capabilities.

CHAPTER TWO: LITERATURE REVIEW

The development of high temperature structural composite materials has been very limited due to the high cost of the materials and the processing required. Polymer matrix composites are popular for structural components because the resins used have low viscosity, allowing complex shapes to be formed prior to curing. However, their use in elevated temperatures is limited; high temperature polymers such as bismaleimides and polyimides have a maximum operating temperature around 300°C. (Mangalgiri, 2005) One study, which exposed bismaliemide composites to 260°C demonstrated a steady state of mass loss, reaching 25% loss after 3000 hours; this correlated with degradation in mechanical properties during bend testing. (Hague et al., 2014)

Ceramic materials operate at much higher temperatures but are more expensive to produce in bulk volumes than polymer matrix derivatives. The primary methods of producing a continuous fiber reinforced ceramic matrix composite are chemical vapor infiltration, reactive melt infiltration, slurry impregnation and hot pressing, and polymer infiltration and pyrolysis. Chemical vapor deposition uses a gaseous precursor and diffuses it into the fiber preform. This allows for deposition of the matrix at the nanometer-scale, but it is relatively slow. The other three methods use a liquid precursor, which is optimal for making structural components as the quicker infiltration of the matrix allows the formation of larger shapes in a reasonable time period. Reactive melt infiltration requires the matrix material to melt in order to penetrate the fiber form. This requires the elements in the matrix to have low melting temperatures or else the fibers are at risk for damage. For slurry impregnation and hot pressing, the fiber form is impregnated with a slurry and put into a hot press, which could potentially damage the fiber.

Polymer infiltration and pyrolysis (PIP) begins with a polymer precursor which is combined with the fibers and cured in an oxygen environment to allow for crosslinking, which inhibits any further shape changes. The part is then pyrolized at high temperatures in an inert environment, removing the polymer chains and leaving the ceramic backbone. The part then requires reinfiltration with the polymer and further pyrolysis cycles in order to increase the density of the ceramic matrix which maximizes the ceramic content and increases the strength. (Naslain, 1999)

Although carbon fibers are typically used for aerospace applications, basalt fibers have been receiving more attention due to their strength, temperature capabilities, and the abundance of basalt on Earth as well as other planetary bodies, making these fibers attractive for future aerospace applications. Continuous basalt fibers are becoming more readily available in a variety of fabric styles. The combination of basalt with polymer derived ceramics is an area of composites which has seen little research to date but is becoming more popular.

<u>Polymer Derived Ceramics</u>

Several polymers have been studied as a polymer derived ceramic (PDC) for PIP processing. Polysiloxanes, polycarbosilanes, and polysilazanes can all be pyrolized to form silicon carbide. Polysiloxanes (PSX) contain a Si-O-C, or silicon oxycarbide, backbone when pyrolized up to 1000°C. Figure 4 shows the basic structure of polysiloxane. Polysiloxanes are relatively inexpensive in comparison to other PDCs, but it requires higher pyrolysis temperatures in order to obtain silicon carbide.
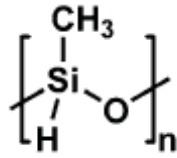
Figure 4 Structure of a Linear Polysiloxane (Torrey et al., 2006)

A study by Gumula *et. al*. in 2009 examined four PSX resins with varying ratios of carbon to silicon. These variations were compared to the mass loss as the polymer was pyrolized to a silicon carbide, SiC, from 1000° to 1700°C. This study concluded that a 1:1 ratio produced the lowest mass loss, but it was also the only sample to remain as a silicon oxycarbide at 1700°C, while the others had converted to silicon carbide. (Gumula, Paluszkiewicz, & Blazewicz, 2009) A follow-up study in 2013 examined the effects of adding continuous carbon fibers to the polymer. The results of this testing indicated that the addition of carbon fibers caused an increase in mass loss at 1700°C. The authors suggest that an increase in the surface area at the matrix/fiber interface affects the conversion of the matrix, which increases the gasses produced and the pores that develop. (Gumula & Blazewicz, 2013)

Polycarbosilane, an organosilicon polymer, contains a silicon-carbon backbone, as shown in Figure 5. Work with polycarbosilanes began in the 1970s under Yajima, who developed silicon carbide continuous fibers. (YAJIMA et al., 1976) Curing polycarbosilane turns the Si-H and Si-CH$_3$ bonds into Si-O-Si and Si-O-C due to oxidation. Alteration of the curing conditions, such as ramp rate, curing temperature, and dwell time, affect how much oxidation occurs. A study by Ly et. al. found that a slower ramp rate, less than 0.5°C/min, and longer curing time, around 1.5 hours at 200°C, increases the amount of crosslinking. (Ly, Taylor, & Day, 2001a)

During the pyrolysis, the resin forms a Si-O-C phase; around 1200°C, β-SiC begins to crystallize. This is similar to the pyrolysis of the polysiloxane, except that the transformation to β-SiC occurs at a lower temperature. A follow up study by Ly et. al. found that pyrolyzing uncured polycarbosilane resulted in β-SiC crystallization at even lower temperatures, around 1000°C. (Ly et al., 2001b) Therefore, curing and pyrolization methods can be adjusted to get the optimal properties needed for the application.
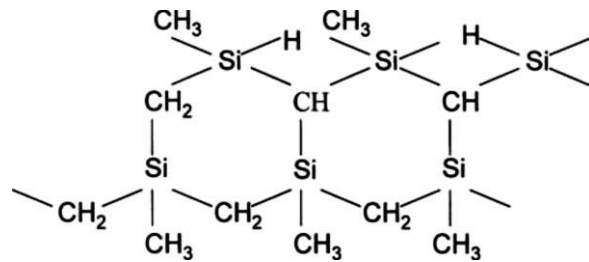
Figure 5 Polycarbosilane Structure (Ly et al., 2001a)

Several studies have researched carbon fiber reinforced ceramic matrix composites, but only a few have looked at the PIP process using polycarbosilane reinforced with carbon fiber. One study compared the microstructure of two carbon fibers and the effects of how they bonded to the resin and transformed during pyrolysis. For ceramic matrix composites, the flexural strength is increased when the fibers are weakly bonded to the matrix and instead absorb energy through the friction between the fiber and the matrix. When the bond is strong, the fibers have a brittle failure that occurs at the same loading as the matrix; this prevents the fibers from serving as a reinforcement. (Zheng et al., 1999) Another study tested the flexural strength of carbon fiber reinforced polycarbosilane composites. It found the strength to be 27 MPa and the failure to be less brittle than monolithic ceramics. (Nicholas et al., 2012)

14

<center>Continuous Basalt Fiber</center>

Basalt is a naturally occurring material found in volcanic rock. Although the use of basalt in structural and high temperature applications has been under development for over 50 years, only in the past decade has there been an emergence of published research on the incorporation of basalt fibers as reinforcement in composites. Carbon fibers are widely used because of their high thermal and mechanical properties, but they are expensive. Glass fibers are less expensive, but have a lower operating temperature than carbon fibers. Basalt fibers are around the same cost as glass fibers, but they have a higher operating temperature and slightly higher mechanical and thermal properties as presented in Table 3. (Singha, 2012) This makes basalt an ideal choice for consideration as an alternative to glass and carbon as reinforcement.

<center>**Table 3. Comparison of Glass Fiber to Basalt Fiber**</center>

	E-Glass Fiber	Basalt Fiber
Maximum Operating Temperature (deg C)	480	800
Average Strength (Mpa)	3400	4000
Average Density (kg/m^3)	2500	2700
Average Thermal Conductivity (W/m-K)	0.037	0.035

The composition of the basalt is very important for both the fabrication and the resulting properties of basalt fibers. Although the exact composition varies depending on the geographical location and the rate of cooling as the molten lava reaches the surface, basalt is composed of three main components. Plagioclase is a series of minerals in the feldspar family. Pyroxene is a group of chain silicates. Olivine is a magnesium iron silicate. (Singha, 2012) Currently, the majority of the basalt used to fabricate continuous basalt fibers comes from the Ukraine and

<center>15</center>

Georgia. When compared with basalt mined from other regions, the differences in the viscosity and melting temperatures affect the fabrication process of long continuous fibers. (A. G. Novitskii & Efremov, 2013) Basalt fiber has an acidity modulus, which is the ratio of acidic to basic oxides, greater than 1.5 which gives it the desired properties such as high strength at elevated temperatures and acoustic dampening. (Czigány, 2005) This high acidity modulus is due a silicon oxide level greater than 46%. (Militky & Kovacic, 2000) The basalt composition found in the Ukraine has a silicon oxide content of greater than 50%, which again leads to these improved properties. (A. G. Novitskii & Efremov, 2013)

Basalt fibers can be formed by either the Junkers method or the spinneret method. The Junkers method uses melt blowing to form short fibers. Long continuous fibers are made using the spinneret method, which uses more precise methods to form and size the fibers. (Singha, 2012) A study on the fabrication of long fibers by Novitskii and Efremov found that the temperature, length of time at the temperature, and the cooling rate all affect the properties of the fiber. Of the two processes for fabricating long fibers compared in this study, the one which held the melt at temperature for a longer period had better properties. (A. Novitskii & Efremov, 2011) A study by Ivanitskii and Gorbachev looked at the fabrication of continuous basalt fibers using the glass fiber fabrication process. Differences in the viscosity, crystallization, and wettability between glass and basalt causes complications and therefore requires many alterations to the glass fiber process in order to fabricate basalt fibers. (Ivanitskii & Gorbachev, 2011) Further research and development into the fabrication process will increase the production of high quality continuous basalt fibers and expand the development and use of these fibers in more widespread applications.

Basalt is a good candidate due to its high elastic modulus, heat resistance, and acoustic dampening. (Czigány, 2005) The literature gives tensile strength values from 1500 to 4000 MPa and operating temperatures around 800°C. Above this, degradation begins to occur. The melting point of basalt is around 1400°C.

Basalt fibers have also been found to perform well after being immersed in various environments. Ying and Zhou compared the tensile strength of basalt fibers and glass fibers after immersion in water, HCl, and NaOH. When in water or HCl, the glass fibers lost strength over time. The basalt fibers had an initial slight decrease in strength, but then there was a period of increased strength, followed by another decrease. The authors suggest that the chemical reactions taking place between the fiber and the water or the HCl caused a protective layer on the fiber, which increased the strength. As the reaction continued over time, the fiber began to degrade, decreasing the strength. The fibers in the alkali solution underwent a chemical change on the fiber surface which caused an immediate decrease in strength. (Ying & Zhou, 2013) Favorable results for immersion in HCl are desirable as HCl exposure can be prevalent in a launch pad environment.

One study looked at the use of basalt fiber composites for fire protection. This study cites the high temperature capabilities and relatively low cost of basalt fibers. A flame test was performed with an oxyacetylene torch. Two configurations were used: one with woven basalt in an epoxy matrix and one with chopped basalt in concrete. Both tests showed better flame resistance than a fiberglass and polyester resin composite panel and another thermal insulative panel. The low thermal conductivity keeps the high temperature from spreading quickly through the panel. (Landucci, Rossi, Nicolella, & Zanelli, 2009)

Because of the high temperature stability of basalt fibers, a series of studies was performed on the mechanical behavior of the fibers alone as well as the effect of partial pyrolysis on a polysiloxane matrix reinforced with basalt fibers. The high temperature tensile properties of basalt fibers were found to be similar to those of glass fibers. (Cerny et al., 2007) This study of basalt fiber reinforcement in a polysiloxane resin conducted pyrolysis at temperatures ranging from 400°C to 800°C. Tensile testing found that the fiber is prone to elongation at temperatures above 600°C and that microcracking in the matrix causes cracking in the fiber as well; the authors suggest that further attention be paid to the processing pressure and temperature rates in to mitigate these effects. The results of the study found that the elastic and shear moduli of the composites increased with oxidative heat treatment, and the authors attribute this to a more complete transformation of the polymer matrix to a ceramic matrix. (Glogar, Sucharda, Cerny, Puchegger, & Peterlik, 2007) Another study performed mechanical testing on unidirectional basalt fiber/polysiloxane composites, looking at both the pyrolysis temperature (650°C or 750°C) and the effect of fiber surface treatment. This study found that the surface treatment and the lower pyrolysis temperature increased the shear modulus but did not have significant effect on the elastic modulus, which is dominated by the fibers. (Glogar et al., 2007) A more recent study tested plain weave basalt fiber/polysiloxane composites at pyrolysis temperatures up to 800°C. The flexural strength of the specimens pyrolized at 450°C only reached 30 MPa. As the pyrolysis temperature was increased to 650°C, the flexural strength increased to slightly above 100 MPa. Above 650°C, there was a slight decrease in the flexural strength. It is suggested that this variation in flexural strength is due to a greater percentage of resin converted to a ceramic matrix. (Cerny et al., 2014)

Thermal and Mechanical Testing of PIP CMCs

Thermal and mechanical testing of fiber reinforced ceramic matrix composites has yielded promising results. Typically, oxyacetylene torch testing is used as it provides a quick study of how the material handles a high heat load. One study performed on PIP processed C/Zr-O-Si-C, using polycarbosilane as the SiC precursor, used bend testing and oxyacetylene torch thermal input to characterize the material. For test panels pyrolized up to 1200°C, the flexural strength was 370.6 MPa and the recession rate during torch testing was 0.0297 mm/sec. (Ma & Chen, 2013)

CHAPTER THREE: FABRICATION

Panel Cure and Pyrolysis

Composite panel fabrication requires the consideration of several factors. The viscosity of the resin and the fiber form used affects the ability of the resin to flow through the fabric, influencing the porosity in the part. The cure cycle is optimized based on the temperature and the time at temperature that the resin is exposed to. The method of fabrication, such as wet layup, resin transfer mold, or preimpregnated fabrics, also affects the outcome of the part.

For this study of ceramic materials for a high temperature application, a polysiloxane and a polycarbosilane were selected, both from Starfire Systems. Material properties provided by Starfire are given in Table 4. Two different basalt fabrics were used, a biaxial fabric from FiberStar and a plain weave fabric from Sudaglass Fiber Technology; material properties are given in Table 5.

Table 4. Properties of PDC Resins

	SPR-688	SMP-10
Density (g/cm^3)	1.11	0.998
Viscosity (cPs at 25 degC)	300-2000	40 to 100
Flash Point (degC)	93	89

Table 5. Properties of Basalt Fabrics

	Biaxial	Plain Weave
Density (g/cm^3)	2.64	2.7
Melting Point (°C)	1050	1350

Curing processes were provided by Starfire for hot press processing; this was used as a basis for the cure cycle, with further direction provided in the study performed on SMP-10 and carbon fibers. (Nicholas et al., 2012) The cure cycle for each of the PDCs was first developed by curing resin only samples; small thin samples using basalt fiber were then cured to ensure an acceptable part could be produced. The final cure cycle used for the test panels is given in Table 6; curing was performed in the autoclave under 28 inHg of vacuum and 20 psi of pressure. Small specimens with six layers of basalt biaxial fabric were fabricated using a wet layup process; this involves applying the resin to each layer of fabric and then stacking them. 2" x 3" specimens were cut from these panels and subsequently pyrolized in a tube furnace. The pyrolysis cycle in the tube furnace is given in Table 6. The hold time at 850°C ranged from 60 minutes to 150 minutes in order to determine the length of time required to obtain the greatest mass loss, which correlates to the most ceramic conversion; it was determined that 90 minutes is the optimal hold time.

Table 6. Cure Cycles

	Polysiloxane	Polycarbosilane
Ramp Up	3°C/min	3°C/min
Hold Temp	100°C	170°C
Hold Time	90 min	90 min
Ramp Down	3°C/min	3°C/min

Larger test panels were then fabricated and pyrolized in an electric ceramic kiln from L&L Kilns. These larger panels require a slower cure process in order to allow for even heat distribution throughout the part. The construction of these 6" x 6" panels consists of polysiloxane and 12 layers of biaxial basalt fabric, resulting in 0.25" thick panels. The polysiloxane panels were able

to be pyrolized with the cycle given in Table 6 with minimal shrinkage, as can be seen in Figure 6.

Table 7. Pyrolysis Cycle for Polysiloxane in Kiln

Ramp Up	1°C/min
Hold Temp	650°C
Ramp Up	2°C/min
Hold Temp	850°C
Hold Time	90 minutes
Ramp Down	5°C/min
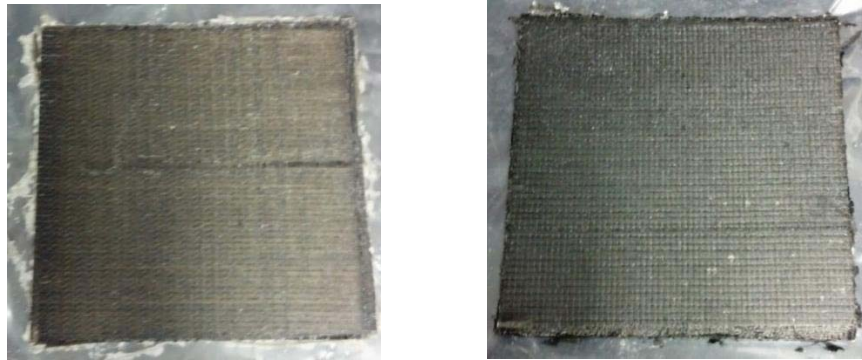
Figure 6. Panel LBF107 after cure (left) and after pyrolysis (right)

The first panels fabricated with polycarbosilane also used this cycle, but all demonstrated bowing of the samples post pyrolysis. In an effort to reduce or eliminate the bowing effect, various cycles were attempted in order to reduce the heat rate and allow the part to heat more evenly. Table 8 shows the cycles used for the polycarbosilane torch testing panels. Figure 7 visually compares one of the polycarbosilane panels after cure and after pyrolysis. Although the shape change is reduced with the reduced heat rates, some curvature in the panels remained.

Table 8. Cure Cycles of Polycarbosilane Panels for Torch Testing

LBF203	LBF204	LBF206	LBF207	LBF208
1°C/min	1°C/min	1°C/min	1°C/min	1°C/min
650°C	200°C	200°C	260°C	650°C
No Hold	60 min	60 min	180 min	No Hold
2°C/min	1°C/min	1°C/min	1°C/min	2°C/min
850°C	400°C	300°C	300°C	850°C
90 min	60 min	60 min	60 min	90 min
-5°C/min	1°C/min	1°C/min	1°C/min	-1°C/min
	600°C	500°C	500°C	
	60 min	60 min	60 min	
	1°C/min	1°C/min	1°C/min	
	700°C	600°C	600°C	
	60 min	60 min	60 min	
	1°C/min	1°C/min	1°C/min	
	850°C	700°C	700°C	
	60 min	60 min	60 min	
	-0.75°C/min	1°C/min	1°C/min	
	350°C	850°C	850°C	
	-1°C/min	60 min	60 min	
	100°C	-0.75°C/min	-0.75°C/min	
		100°C	100°C	
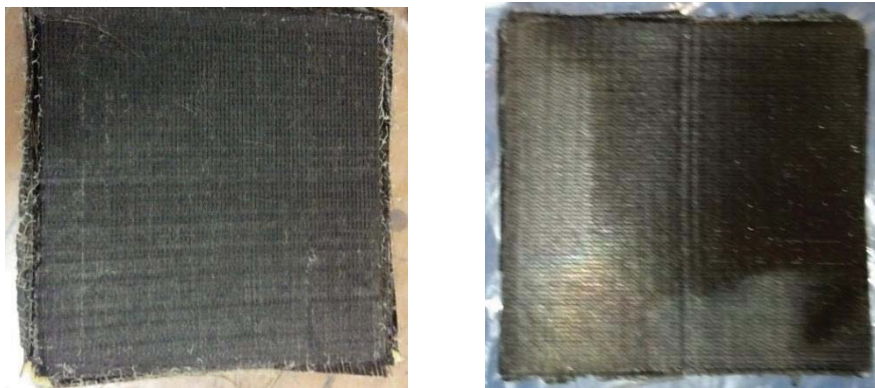
Figure 7. Panel LBF214 after cure (left) and pyrolysis (right)

Five 6" x 6" panels of each PDC were fabricated for the Oxyacetylene Torch Testing.

Table 9 lists fabrication data for the panels. After pyrolysis, the panels shrunk slightly to 5.5" x

5.5". For the polysiloxane panels, the average resin content by mass is 21% and the average resin mass retained after pyrolysis is 71%. For the polycarbosilane panels, the average resin content by mass is 20% and the average resin mass retained after pyrolysis is 84%. Additionally, one panel was made for bend testing; fabrication data is given in Table 10.

Table 9. Fabrication Data

Panel ID	PDC Used	CURED PANEL		PYROLIZED PANELS	
		Fiber Volume Fraction	Resin Content by Weight	Mass Retained	Resin Retained
LBF103	SPR-688 (Polysiloxane)	56.15%	23.45%	94.66%	76.27%
LBF104		52.55%	19.49%	93.20%	69.28%
LBF105		52.11%	21.37%	92.96%	70.54%
LBF106		52.00%	19.35%	93.12%	69.00%
LBF107		52.09%	20.01%	93.09%	69.61%
LBF203	SMP-10 (Polycarbosilane)	54.72%	18.73%	95.51%	76.67%
LBF204		49.48%	19.39%	97.95%	89.41%
LBF206		49.45%	20.88%	97.10%	86.67%
LBF207		49.69%	21.01%	See Note 1	
LBF208		49.59%	19.73%	See Note 1	

Note 1: Post pyrolysis weight was not acquired prior to panel testing; therefore these values were not able to be calculated

Table 10. Fabrication Data for Bend Test Panel #1

Panel ID	PDC Used	POST CURE		POST PYROLYSIS	
		Fiber Volume Fraction	Resin Content by Weight	Mass Retained	Resin Retained
LBF214	SMP-10	43.85%	18.82%	97.78%	88.19%

A second set of polycarbosilane panels was also fabricated using the plain weave basalt fabric. An impregnator was used to apply the resin to the fabric. Each layer of fabric is placed between the impregnator's two rollers which forces the resin into the fabric. This allows for a more even distribution of the resin in the fabric. These panels also received reinfiltration as described below. Table 11 gives the fabrication data for the panels used for oxyacetylene torch testing and Table 12 shows the fabrication data for bend test panel.

<u>Reinfiltration and Pyrolysis Cycles</u>

Voids in the ceramic matrix occur during pyrolysis: these may be filled by reinfiltrating the part with the PDC and then pyrolizing again. Reinfiltration was performed in a cylindrical vacuum chamber from Laco Technologies. The part was covered in resin then placed under vacuum for 90 minutes. After reinfiltration, the part was pyrolized using the parameters if the initial pyrolysis cycle. This process was only performed with polycarbosilane.

Table 11. Fabrication Data for Reinfiltrated Panels

Panel ID	POST CURE		PYROLYSIS		REINFILTRATION #1		REINFILTRATION #2	
	Fiber Volume	Resin Content	Mass Retained	Resin Retained	Resin Retained (%)	Resin Content	Resin Retained (%)	Resin Content
LBF216	57.49%	18.12%	98.26%	89.26%	96.71%	17.52%	96.85%	18.19%
LBF222	55.87%	17.69%	94.89%	71.10%	76.21%	19.01%	79.29%	22.63%
LBF224	55.07%	18.54%	95.34%	74.86%	72.04%	19.26%	83.18%	22.64%
LBF225	54.09%	17.69%	95.28%	73.29%	67.40%	19.09%	77.26%	22.38%

Table 12. Fabrication Data for Bend Test Panel #2

Sample ID	Panel Layup	POST CURE		PYROLYSIS	
		Fiber Volume Fraction	Resin Content by Weight	Mass Retained	Resin Retained
LBF215	[45/0/45/0]s	57.36%	15.10%	99.37%	96.38%
		REINFILTRATION #1		REINFILTRATION #2	
		Resin Retained	Resin Content by Weight	Resin Retained	Resin Content by Weight
		83.85%	19.29%	95.54%	20.12%

CHAPTER FOUR: MATERIAL TESTING METHODS

This study analyzed the material's microstructure, high temperature capability, and mechanical performance. In order to characterize the fiber/matrix interface and the chemical composition, Scanning Electron Microscopy/Energy Dispersive Spectroscopy was performed, as well as X-Ray Diffraction. Thermogravimetric Analysis was also performed on panels. Panels underwent high temperature thermal testing by performing oxyacetylene torch testing. Three point bending was also performed to assess the mechanical performance of the composite.

Scanning Electron Microscopy

Scanning electron microscopy (SEM) was performed using a Zeiss ULTRA 55 Field Emission Gun SEM at the Materials Characterization Facility. This machine also performs Energy Dispersive Spectroscopy (EDS) with a Noran System 7 EDS system with Silicon Drift Detector. SEM uses an electron beam to obtain surface features on a nanoscale. EDS determines the elements in a material by detecting the energy released from atoms as they are hit with an electron beam. Figure 8 shows SEM images of basalt fibers. The image on the left is fibers taken from the biaxial fabric and the one on the right is from the plain weave fabric. The fibers appear to be very similar in shape and size. Figure 9 shows the elemental composition of the fibers from the plain weave basalt. The elements that appear are Carbon, Oxygen, Iron, Sodium, Magnesium, Aluminum, Silicon, Potassium, and Calcium, which are all expected for basalt.
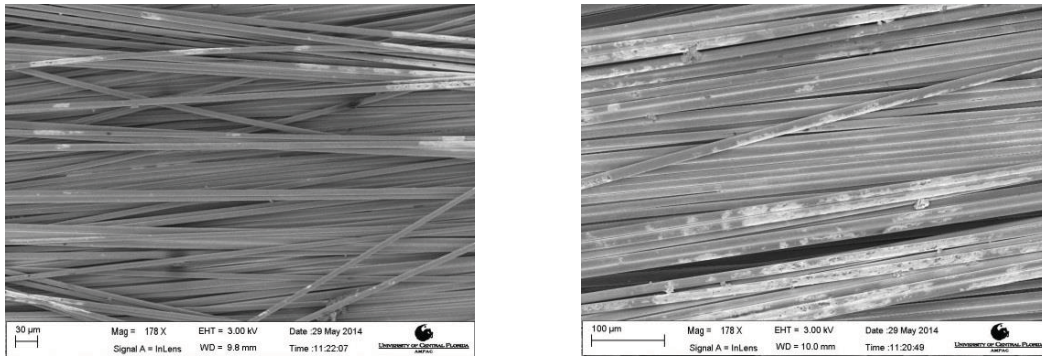
Figure 8. SEM of Biaxial Basalt (Left) and Plain Weave Basalt (Right)
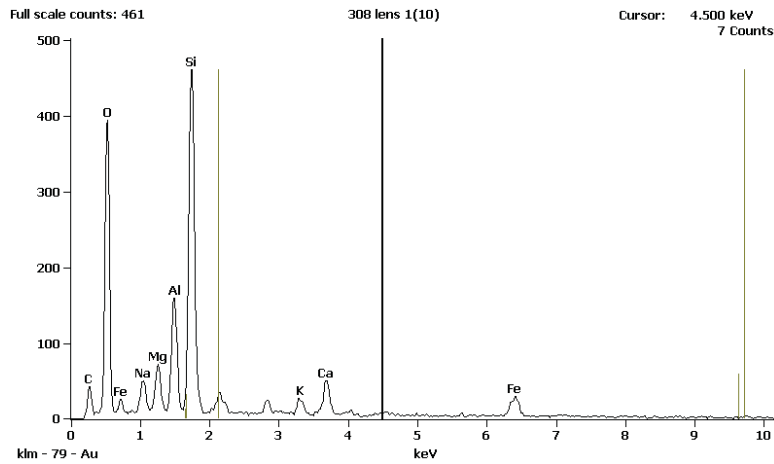
Figure 9. EDS of Plain Weave Basalt Fiber

Figure 10 shows cross sections of polysiloxane panels. The image on the left shows good penetration of the resin into the fiber tow and although this panel only received one pyrolysis cycle, there is a suitable amount of ceramic around the fibers. The image on the right shows the interface between a longitudinal layer and a transverse layer of fibers. Again, we can see an adequate quantity of ceramic around the fibers. EDS of a fiber in the panel, shown in Figure 11, shows all the elements contained in basalt; the gold is due to the gold spattering applied to the

sample to provide electrical conductivity necessary for EDS. Figure 12 shows EDS of the matrix. The main elements are silicon, oxygen, and carbon, which are expected for the temperature at which these parts were pyrolized. The aluminum and calcium are artifacts of the basalt fiber.
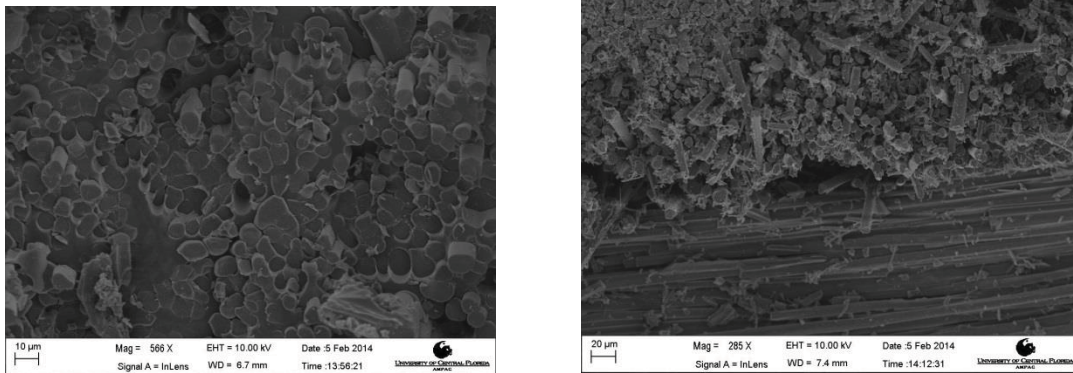
Figure 10. SEM Images of Polysiloxane Panels: LBF105 (Left), LBF107 (Right)
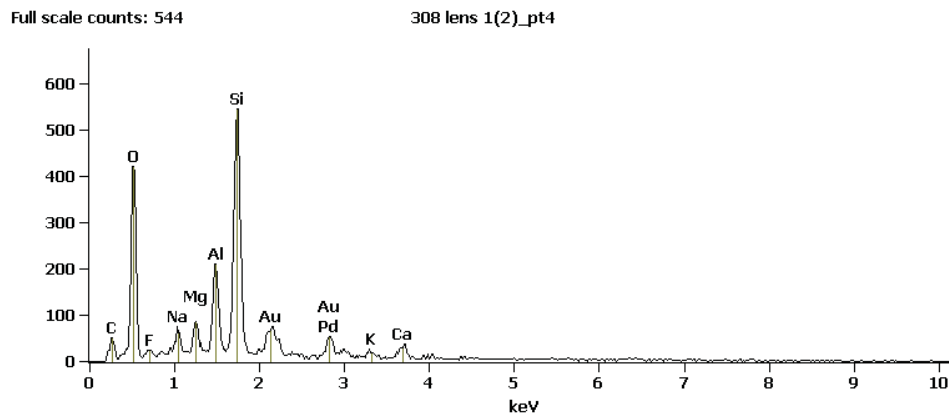
Figure 11. EDS of Fiber from Panel LBF105
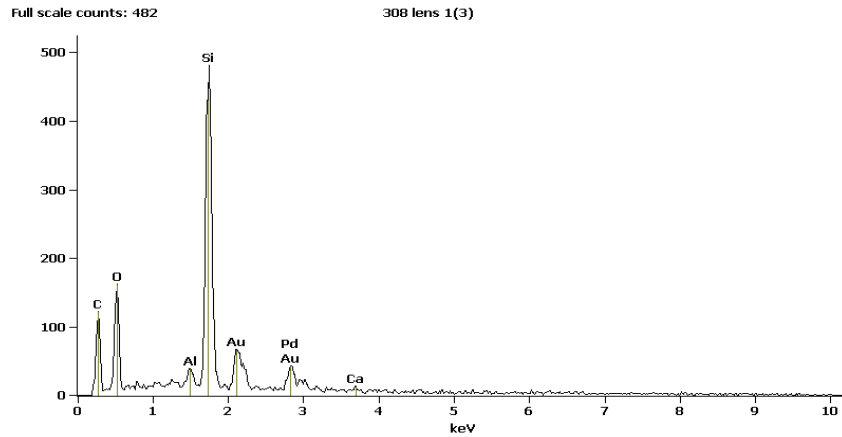
Figure 12. EDS of Matrix Material from Panel LBF105

Figure 13 shows SEM images of the first set of polycarbosilane panels. The image on the left shows voids in the matrix surrounding the fibers, and the image on the right also shows voids within a layer but no significant voids between the layers. Figure 14 and Figure 15 show similar compositions of the polycarbosilane as Figure 12 shows for the polysiloxane panels.
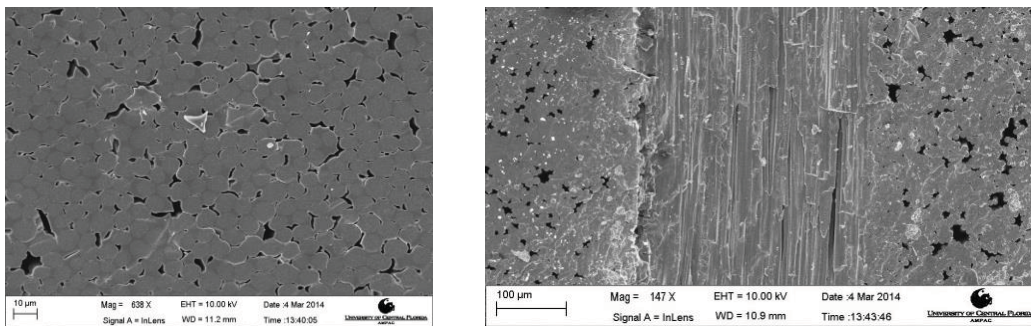
Figure 13. SEM Images of Polycarbosilane Panels: LBF208 (Left). LBF207 (Right)
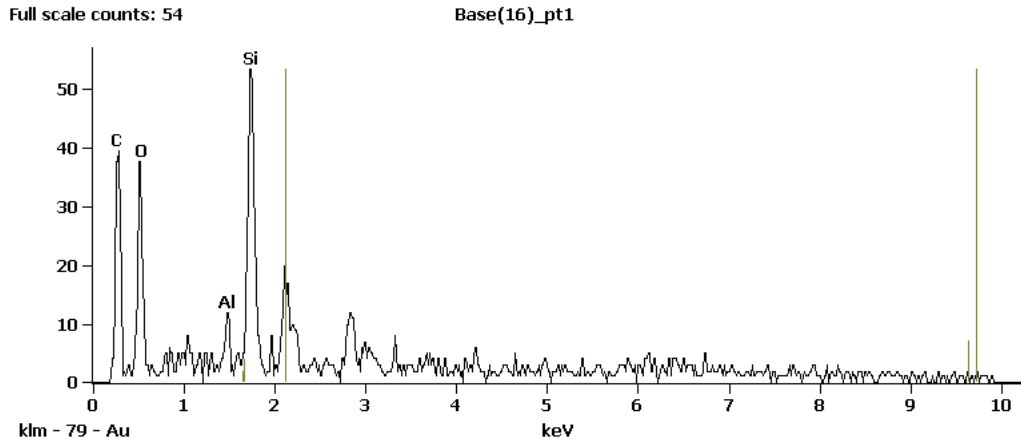
Figure 14. EDS of Matrix Material from Panel LBF214
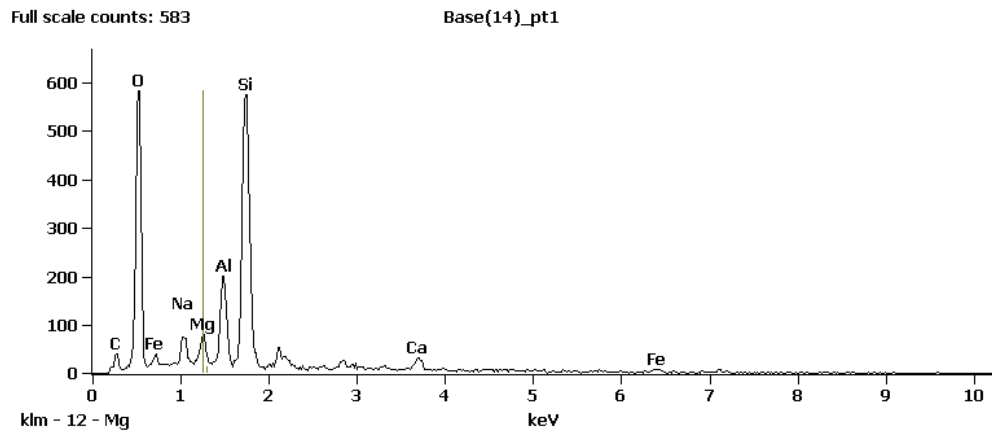
Figure 15. EDS of Fiber from Panel LBF208

Figure 16 and Figure 17 are SEM images of polycarbosilane panels which were pyrolized to 700 °C and reinfiltrated/pyrolized twice. Because these panels are made with plain weave fabric, the fibers are interwoven, giving a different appearance than the stacks of longitudinal and transverse fibers shown in the previous SEM images. In Figure 16, the image demonstrates good contact and few voids between the layers. Figure 17 shows no voids in the interface between the fibers and the

matrix. The elements in Figure 18 represent both the matrix and fiber, both of which contain a high

percentage of silicon.
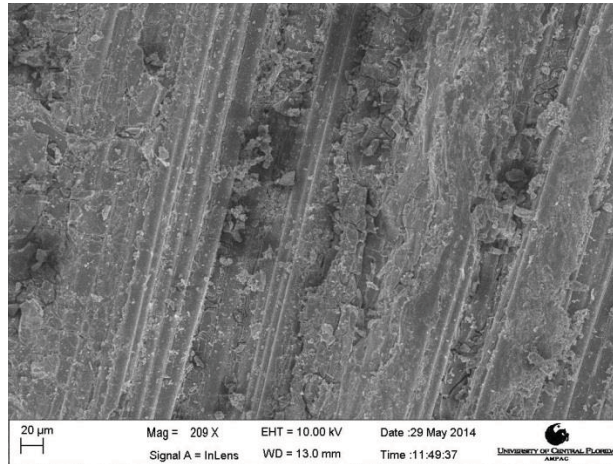
Figure 16. SEM Image of LBF224
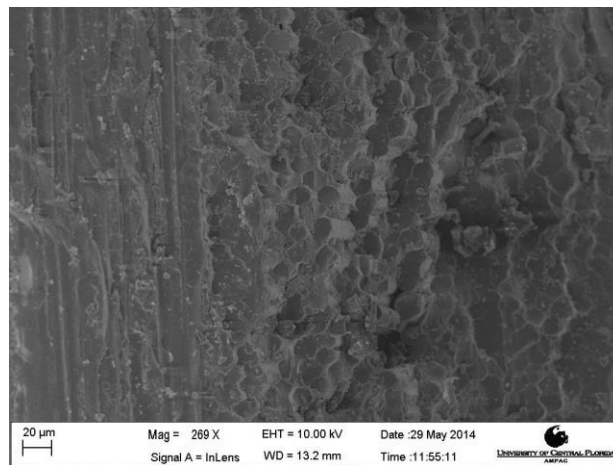
Figure 17. SEM Image of LBF225
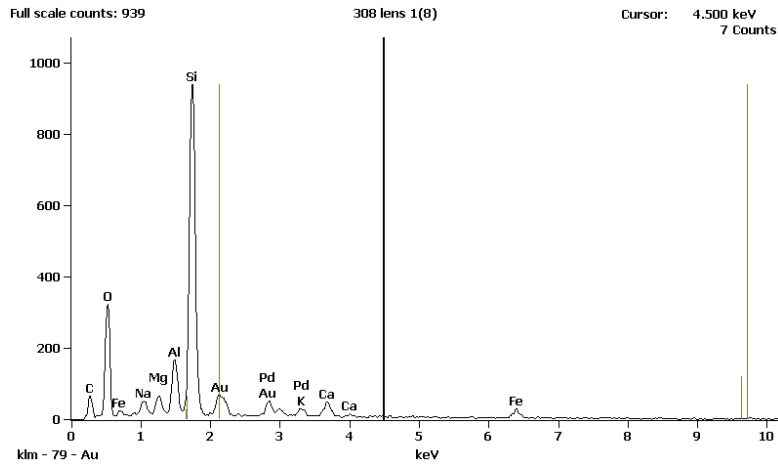
Figure 18. EDS of Panel LBF225

X-Ray Diffraction

X-Ray Diffraction (XRD) is used to determine the crystal structure based on the angles that the x-rays hit the planes of atoms in the material. XRD was performed by a Rigaku D /MAX XRD on a powder sample from Panel LBF225, which was made with the plain weave fabric and polycarbosilane resin and was reinfiltrated twice. Figure 19 confirms that the ceramic matrix is Silicon Carbide, as the peaks from the sample correlate to the peaks in the standard. The waviness in the line is due to the fact that the material is amorphous and not crystalline.
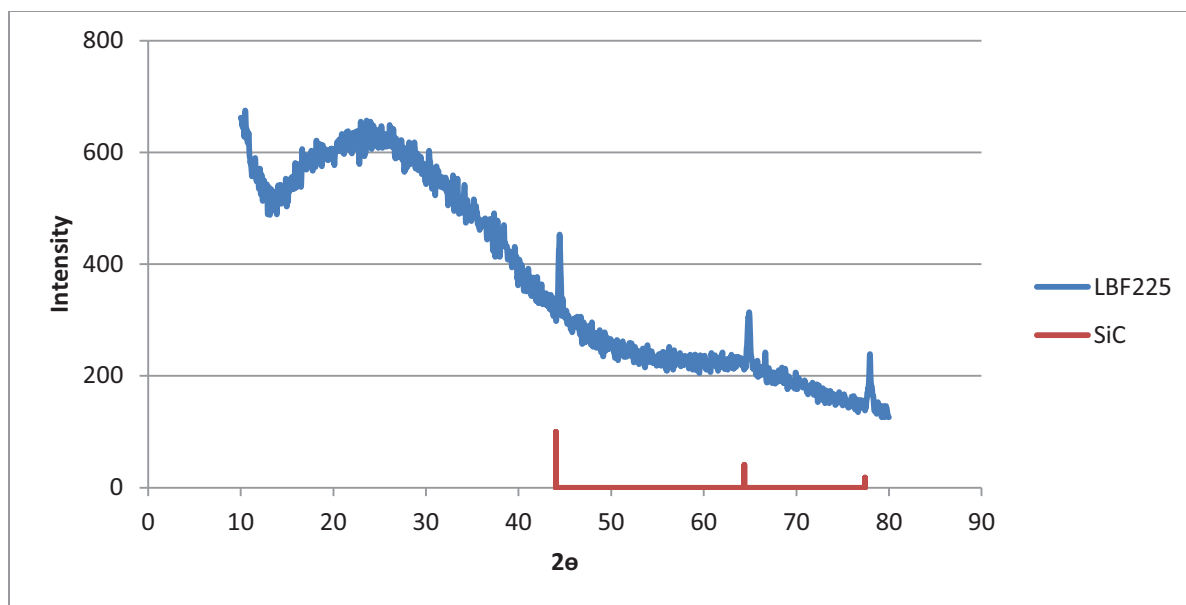
Figure 19. XRD of Panel LBF225

Thermogravimetric Analysis

Thermogravimetric analysis (TGA) is a technique which measures the mass of a specimen as it is heated. TGA was performed by a TA Instruments Q5000 IR instrument. Specimens from three panels were tested, as shown in Figure 20, Figure 21, and Figure 22. There is less than 2% mass loss up to 700°C, which is expected since the panels were pyrolized up to this temperature.
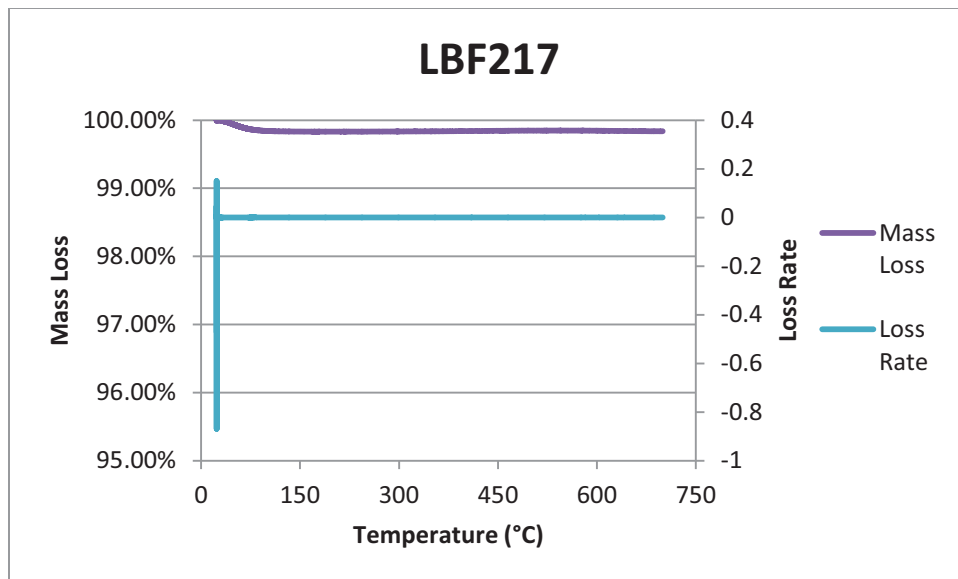
Figure 20. TGA of Panel LBF217
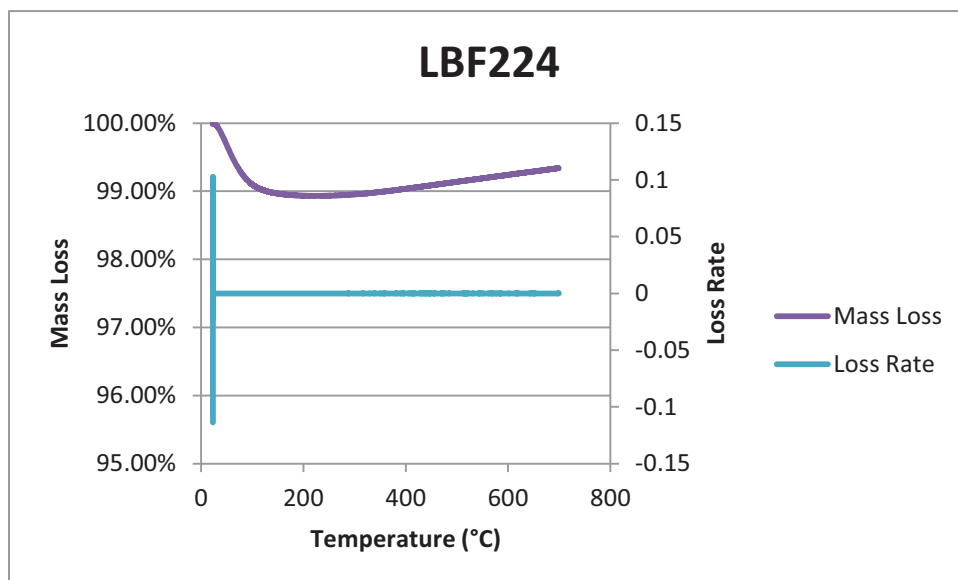
Figure 21. TGA of Panel LBF224
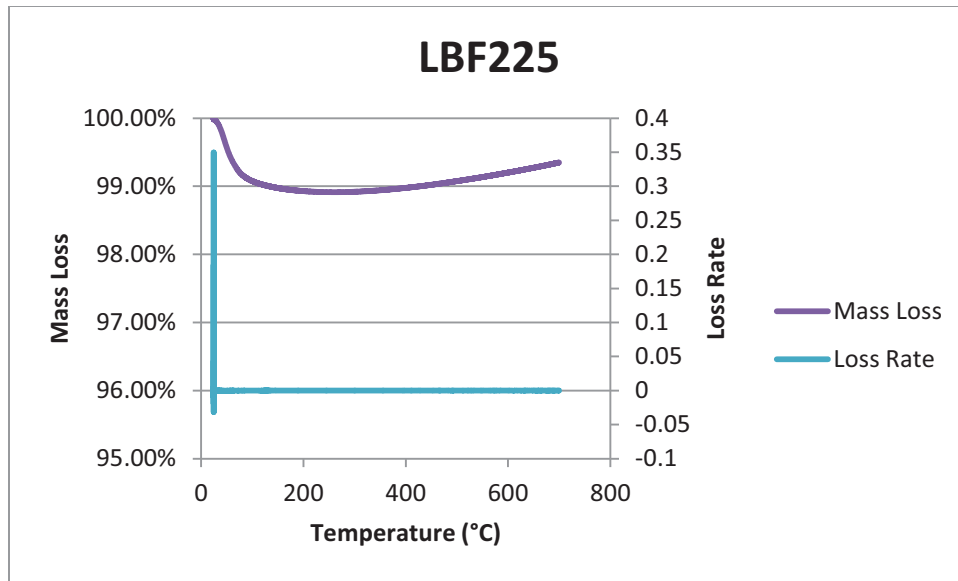
Figure 22. TGA of Panel LBF225

Oxyacetylene Torch Testing

Oxyacetylene torch testing was performed on 5 panels of each of the PDCs which received

pyrolysis only (Table 9) as well as a set of polycarbosilane panels which were

reinfiltrated/pyrolized (Table 11). The testing closely followed the ASTM E285 Method, except

there was no temperature reading for the front of the panel. The panels were trimmed to sample

dimensions of 4" x 4" panels. In the testing set up in Figure 23, the panel is clamped inside a

metal frame which is bolted together, and a thermocouple is bonded to the center of the back of

the panel. A metal cover is placed in front of the panel until the flame is ignited and focused.

Once the flame is ready, the cover moves to the side and the panel slides forward on the rail,

placing it ¾" from the nozzle, as shown in Figure 24. The thermocouple data is recorded for the

duration of the test.
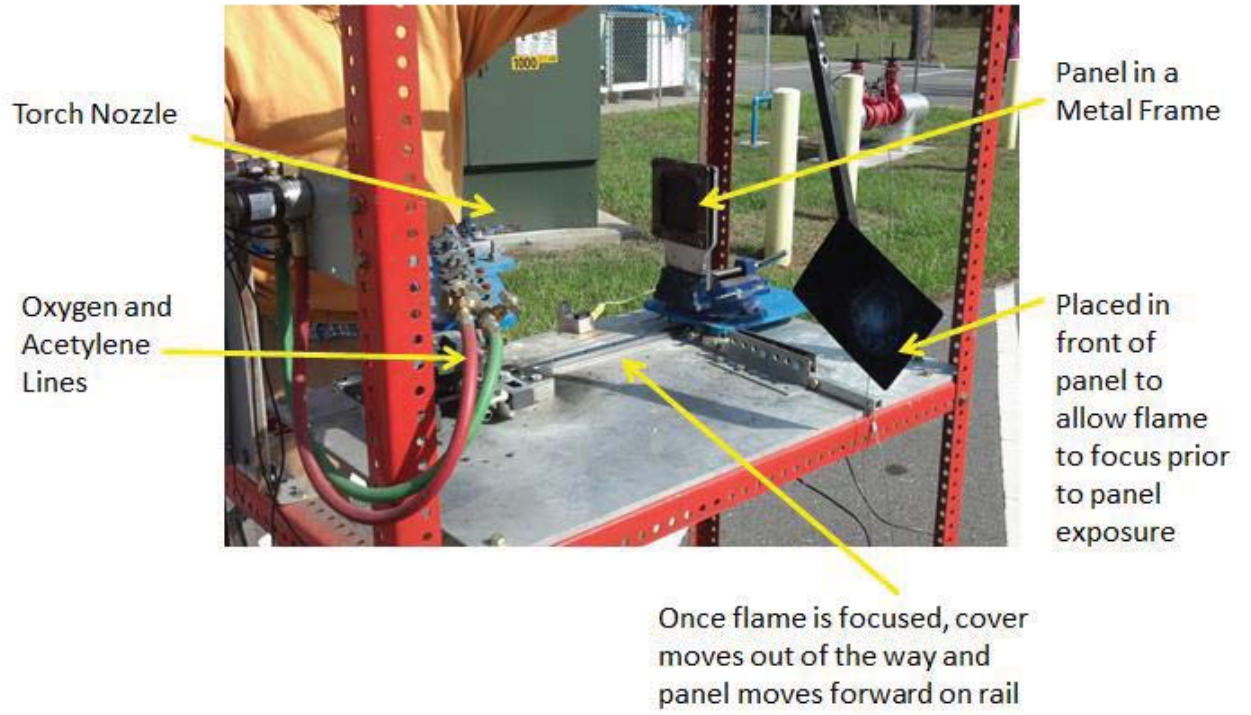
Figure 23. Torch Test Setup

Figure 24. During Test

<u>Flexural Testing</u>

Bend testing was performed referencing ASTM C1341. This test is specifically for three and four point bending of continuous fiber reinforced ceramic composites. Testing was performed on an Instron machine in the Mechanical Engineering Lab as shown in Figure 25. Panel LBF214 (Table 10) was cut into (8) 19 mm wide specimens and three point bending was performed on those specimens with a span to thickness ratio of 24:1. Panel LBF215 (Table 12) was cut into (5) 15 mm wide specimens and three point bending was performed with a span to thickness ratio of 32:1. The flexural strength is calculated using equation (1), where P_U is the maximum load, L is the support span length, b is the specimen width, and d is the specimen thickness.

$$S = \frac{3P_U L}{2bd^2}$$ (1)

Figure 25. 3 Point Bend Test Setup

CHAPTER FIVE: RESULTS AND DISCUSSION

Oxyacetylene Torch Testing of Baseline Panels

Figure 26 and Table 13 list the results of the polysiloxane panel testing. Burnthrough occurred approximately 30-35 seconds into the test. The maximum temperature that was seen by the back face prior to burn through was 180°C. LBF106 and LBF107 had the thermocouple slightly off center, which resulted in lower measured values but still followed the general trend. Figure 27 and Figure 28 show examples of the panels after testing. The front of the panel demonstrates melting and ablation due to the flame. From the back of the panel, a small hole is shown where burnthrough occurred; the region around the hole is melted adhesive that was used to hold on the thermocouple. The side of the panel shows delamination; this is due to lower strength in this direction.
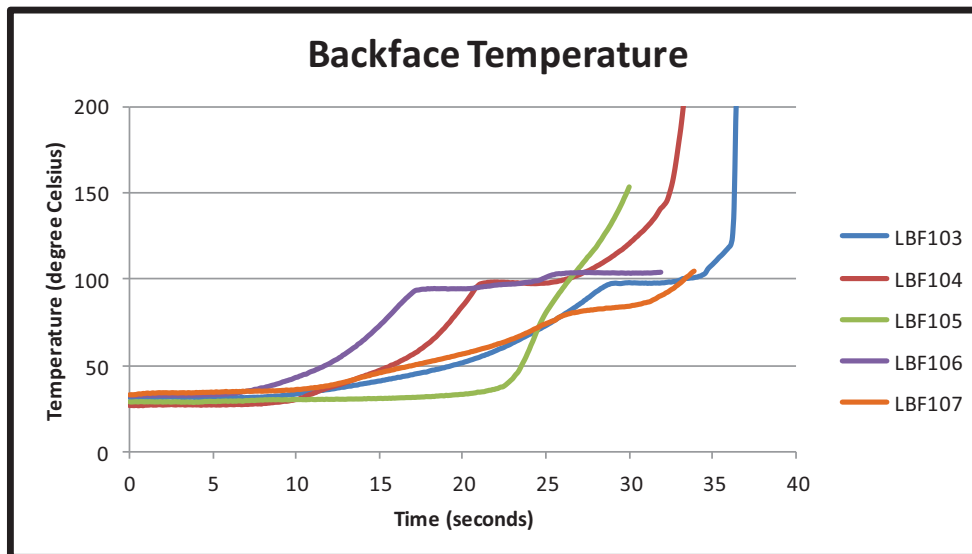
Figure 26. Torch Testing Results of the Polysiloxane Panels

Table 13. Recession Rates for Polysiloxane Panels

PANEL ID	Erosion Rate (mm/sec)
LBF103	0.1868
LBF104	0.1814
LBF105	0.2117
LBF106	0.2048
LBF107	0.1924
AVERAGE	**0.1954**

LBF103 Front of Panel   LBF103 Back of Panel   LBF103 Side of Panel

Figure 27. Panel LBF103 Post Test

LBF106 Front of Panel   LBF106 Back of Panel   LBF106 Side of Panel

Figure 28. Panel LBF106 Post Test

Figure 29 and Table 14 list the results for the polycarbosilane panels. Only panel LBF203 burned through at the impingement point; it took 40 seconds and the backface reached a temperature of 500°C. The other panels were tested until the adhesive holding the thermocouple melted. Because these panels were slightly bowed, there may have been heat intrusion in the gap between the metal frame and the panel. This may have allowed heat to reach the back of the panel from the sides rather than through the panel, which prematurely melted the adhesive. Also, because the panels bowed outward, the impingement point was slightly closer than ¾" which may have changed the heat flux seen by the front of the panel. Even with the early thermal termination, the testing continued for 40-60 seconds, outlasting the polysiloxane panels. Figure 30 shows the panel which did burn through, and Figure 31 is an example of the other panels. These panels cracked through the thickness very early into the test (may be seen in the back face and side views); this is most likely due to the stress on the bowed panels in the frame. The ablation appears to be slightly different than what was seen with the polysiloxane panels and this may be from the bowing in the panel which made the impingement point closer to the panel.
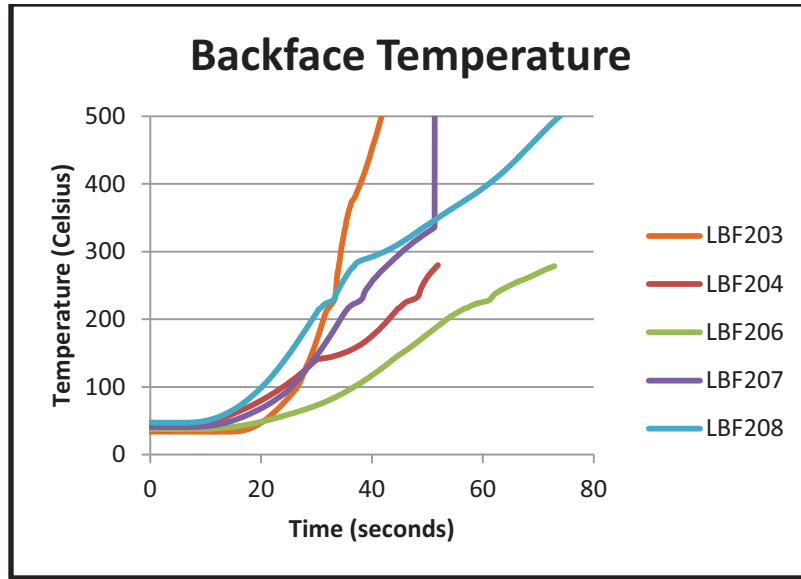
Figure 29. Torch Testing Results of the Polycarbosilane Panels

Table 14. Recession Rates for Polycarbosilane Panels

PANEL ID	Erosion Rate (mm/sec)
LBF203	0.1411
LBF204	0.1323
LBF206	0.1351
LBF207	0.1270
LBF208	0.0635
AVERAGE	**0.1198**

42

Figure 30. Panel LBF203 Post Test

Figure 31. Panel LBF206 Post Test

Oxyacetylene Torch Testing of Reinfiltrated Panels

Figure 32 and Table 15 contain the results for the second set of polycarbosilane panels which were reinfiltrated. LBF216 cracked immediately due to the sudden stop of the frame as it slid forward on the rail towards the torch nozzle, which allowed the heat to go through the panel instantly. All of these panels had burn through times of only 10-13 seconds, which is much less than even the polysiloxane panels. Figure 33 shows one of the panels after the torch test. All the panels

cracked through the thickness, but these did not show interlaminar delamination. The posttest condition of these panels appears similar to the condition of the first set of polycarbosilane panels, except the hole at the impingement point appears bigger on these panels.
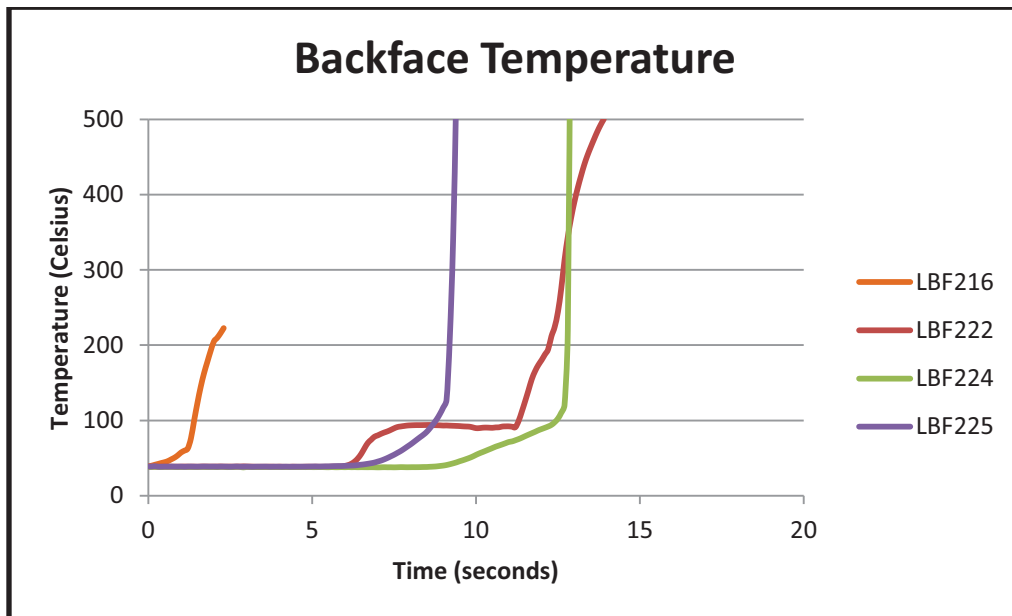
Figure 32. Torch Testing Results of the Reinfiltrated Panels

Table 15. Recession Rates of Reinfiltrated Panels

PANEL ID	Erosion Rate (mm/sec)
LBF216	0.5773
LBF222	0.3735
LBF224	0.3342
LBF225	0.3175
AVERAGE	**0.4006**
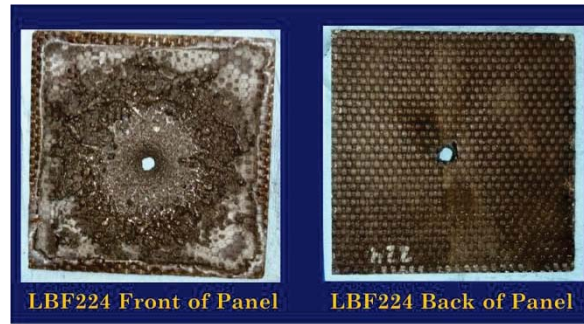
Figure 33. Panel LBF224 Post Test

The decreased burnthrough time could have been a result of the change in the fabric form (the first set was biaxial, the second set was plain weave), or it could have been due to the interface between the fiber and the matrix after reinfiltration. Changes in the test setup, such as the thermocouple attachment technique and a possible slight variation in the heat flow from the torch, could have also affected the results.

Flexural Testing of Baseline Panel

The first panel tested received only one pyrolysis cycle and no reinfiltration. It was then cut into (8) 19 mm wide specimens. The specimens were 6 mm thick and tested at a span of 152 mm, which results in a thickness to span ratio of 24:1. The specimens were loaded at a rate of 0.041mm/min. Figure 34 demonstrates an example of a failed specimen with a crack through the thickness. Figure 35 shows the load vs. the displacement for all 8 specimens. There is very little displacement before failure, which is common for ceramic materials. The fibers in the part allow for more flexure which increases the overall strength. Table 16 lists the calculated flexural strength in each specimen; the average strength is 33.2 MPa
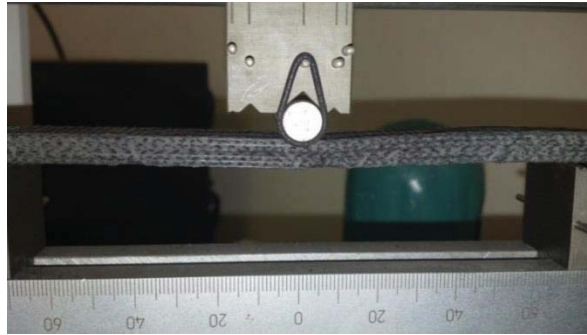
Figure 34. Panel at Failure
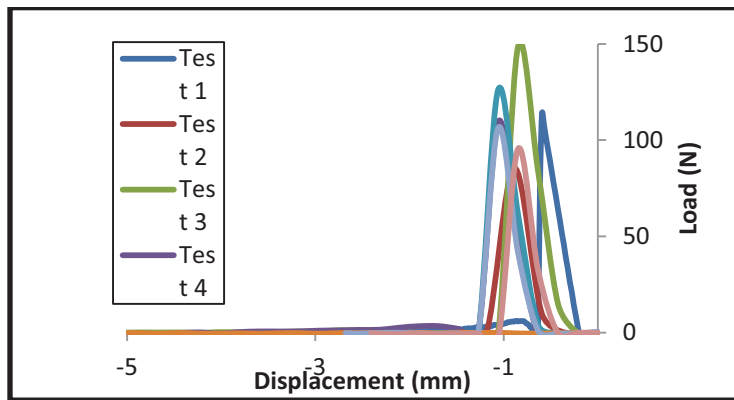
Figure 35. Bending Load vs. Displacement for Polycarbosilane Panel

Table 16. Flexural Strength Data for Polycarbosilane Panel

TEST	MAX LOAD (N)	Strength (MPa)
1	113.88	33.98
2	85.59	25.54
3	148.60	44.34
4	109.52	32.68
5	126.12	37.63
6	104.33	31.13
7	106.34	31.73
8	95.49	28.49

46

Flexural Testing of Reinfiltrated Panel

The second panel tested was reinfiltrated and pyrolized twice to increase the ceramic content. This panel was then cut into (5) 15 mm wide specimens for testing. The specimens were 4 mm thick and tested at a span of 128 mm, resulting in a thickness to span ratio of 32:1. The specimens were tested at a rate of 0.0594 mm/min. Figure 36 shows the displacement vs. load for each specimen. Table 17 lists the flexural strength results with an average of 16.3 MPa.
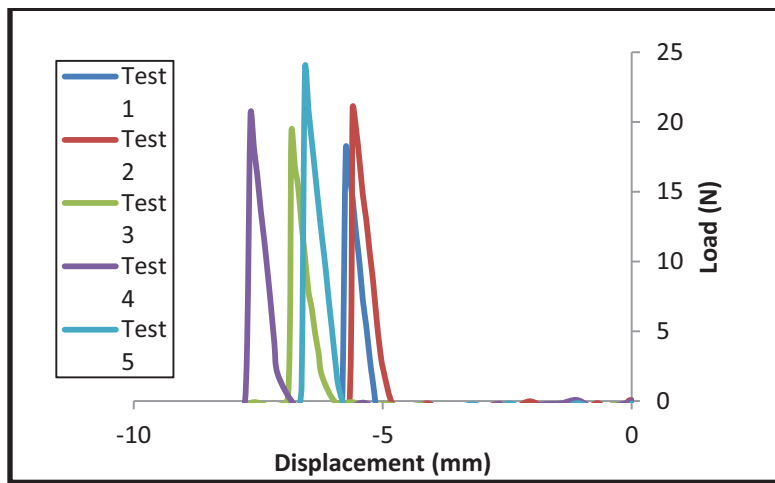
Figure 36. Bending Load vs. Displacement for Reinfiltrated Panel

Table 17. Flexural Strength Data for Reinfiltrated Panel

TEST	MAX LOAD (N)	Flexural Strength (MPa)
1	18.09	14.36
2	21.00	16.66
3	19.26	15.29
4	20.52	16.29
5	23.79	18.88

The reinfiltrated specimens have approximately half of the flexural strength of the pyrolysis only specimens. This could be due to differeing span to thickness ratios, or the increased crosshead speed used for the reinfiltrated panels. It could also be because a different fabric form was used, or the reinfiltration cycles strengthened the bond between the fibers and the matrix causing the fibers to fail in a brittle manner.

CHAPTER SIX: CONCLUSIONS

Ceramic matrix composites are becoming available in more forms. By using a polymer derived ceramic, panels can be fabricated, cured, and then pyrolized to obtain a ceramic matrix in a bulk, structural component. The material characterization showed that the polycarbosilane resin did transform to silicon carbide during pyrolysis. Basalt fiber was chosen for reinforcement due to its thermal and mechanical properties and its availability.

The only available data for a launch environment is for the Space Shuttle. This is a much more extreme environment than what this material is being designed for. The torch testing was performed at a lower heat rate than what was experienced by the Shuttle Launch Pad, but the heat rate at the pad only lasts for a few seconds. During the torch testing, the panels which received only one pyrolysis cycle did not detect heat at the back face of the panels until 10-20 seconds into the test. The reinfiltrated panels had a much shorter burnthrough time. The flexural strength of the reinfiltrated specimens is half of the strength of the specimens which only went through one pyrolysis cycle; both sets of specimens had higher flexural strength than the refractory concrete.

The testing performed show that basalt fiber reinforced ceramic matrix composites are a viable option for high temperature structural applications. The decrease in thermal resistance and flexural strength of the reinfiltrated panels is an area that will require further investigation. It may be because of changes in the basalt fiber or changes in the bond between the fibers and the ceramic matrix. The SEM images show a stronger bond, which causes the fibers to break in a more brittle manner and does not increase the strength of the ceramic. More testing will be required to fully understand the phenomena taking place.

APPENDIX A: PANEL FABRICATION DATA

PANEL LBF103

Table 18. Materials for LBF103

MATERIALS					
Resin	Resin Weight (g)	Fiber	Layup	Fiber Weight (g)	Total Weight (g)
SPR-688	61.00	Biaxial Basalt Fiber	[0/90]11	190.00	251.00

Table 19. Cure Cycle for LBF103

CURE CYCLE	
Ramp Up	3°C/min
Hold Temp	100°C
Hold Time	90 min
Vacuum	-28 inHg
Pressure	20 psi
Post Cure Temp	275°C
Post Cure Hold	24 Hours

Table 20. Post Cure for LBF103

POST CURE		
Weight (g)	Fiber Volume Fraction	Resin Content by Weight
248.20	56.15%	23.45%

Table 21. Pyrolysis Cycle for LBF103

PYROLYSIS CYCLE	
Ramp Up	1°C/min
Hold Temp	650°C
Hold Time	No Hold
Ramp Up	2°C/min
Hold Temp	850°C
Hold Time	90 minutes
Ramp Down	5°C/min

Table 22. Post Pyrolysis for LBF103

PYROLYSIS		
Initial Weight (g)	Post Weight (g)	Resin Retained (%)
245.20	232.10	76.27%

PANEL LBF104

Table 23. Materials for LBF104

MATERIALS					
Resin	Resin Weight (g)	Fiber	Layup	Fiber Weight (g)	Total Weight (g)
SPR-688	81.60	Biaxial Basalt Fiber	[0/90]12	219.80	301.40

Table 24. Cure Cycle for LBF104

CURE CYCLE	
Ramp Up	3°C/min
Hold Temp	100°C
Hold Time	90 min
Vacuum	-28 inHg
Pressure	20 psi
Post Cure Temp	275°C
Post Cure Hold	24 Hours

Table 25. Post Cure for LBF104

POST CURE		
Weight (g)	Fiber Volume Fraction	Resin Content by Weight
273.00	52.55%	19.49%

Table 26. Pyrolysis Cycle for LBF104

PYROLYSIS CYCLE	
Ramp Up	1°C/min
Hold Temp	650°C
Hold Time	No Hold
Ramp Up	2°C/min
Hold Temp	850°C
Hold Time	90 minutes
Ramp Down	5°C/min

Table 27. Post Pyrolysis for LBF104

PYROLYSIS		
Initial Weight (g)	Post Weight (g)	Resin Retained (%)
282.30	263.10	69.28%

PANEL LBF105

Table 28. Materials for LBF105

MATERIALS					
Resin	Resin Weight (g)	Fiber	Layup	Fiber Weight (g)	Total Weight (g)
SPR-688	81.60	Biaxial Basalt Fiber	[0/90]12	216.00	297.60

Table 29. Cure Cycle for LBF105

CURE CYCLE	
Ramp Up	3°C/min
Hold Temp	100°C
Hold Time	90 min
Vacuum	-28 inHg
Pressure	20 psi
Post Cure Temp	275°C
Post Cure Hold	24 Hours

Table 30. Post Cure for LBF105

POST CURE		
Weight (g)	Fiber Volume Fraction	Resin Content by Weight
274.70	52.11%	21.37%

Table 31. Pyrolysis Cycle for LBF105

PYROLYSIS CYCLE	
Ramp Up	1°C/min
Hold Temp	650°C
Hold Time	No Hold
Ramp Up	2°C/min
Hold Temp	850°C
Hold Time	90 minutes
Ramp Down	5°C/min

Table 32. Post Pyrolysis for LBF105

PYROLYSIS		
Initial Weight (g)	Post Weight (g)	Resin Retained (%)
283.90	263.90	70.54%

PANEL LBF106

Table 33. Materials for LBF106

MATERIALS					
Resin	Resin Weight (g)	Fiber	Layup	Fiber Weight (g)	Total Weight (g)
SPR-688	81.60	Biaxial Basalt Fiber	[0/90]12	215.00	296.60

Table 34. Cure Cycle for LBF106

CURE CYCLE	
Ramp Up	3°C/min
Hold Temp	100°C
Hold Time	90 min
Vacuum	-28 inHg
Pressure	20 psi
Post Cure Temp	275°C
Post Cure Hold	24 Hours

Table 35. Post Cure for LBF106

POST CURE		
Weight (g)	Fiber Volume Fraction	Resin Content by Weight
266.60	52.00%	19.35%

Table 36. Pyrolysis Cycle for LBF106

PYROLYSIS CYCLE	
Ramp Up	1°C/min
Hold Temp	650°C
Hold Time	No Hold
Ramp Up	2°C/min
Hold Temp	850°C
Hold Time	90 minutes
Ramp Down	5°C/min

Table 37. Post Pyrolysis for LBF106

PYROLYSIS		
Initial Weight (g)	Post Weight (g)	Resin Retained (%)
276.30	257.30	69.00%

PANEL LBF107

Table 38. Materials for LBF107

MATERIALS					
Resin	Resin Weight (g)	Fiber	Layup	Fiber Weight (g)	Total Weight (g)
SPR-688	81.60	Biaxial Basalt Fiber	[0/90]12	215.80	297.40

Table 39. Cure Cycle for LBF107

CURE CYCLE	
Ramp Up	3°C/min
Hold Temp	100°C
Hold Time	90 min
Vacuum	-28 inHg
Pressure	20 psi
Post Cure Temp	275°C
Post Cure Hold	24 Hours

Table 40. Post Cure for LBF107

POST CURE		
Weight (g)	Fiber Volume Fraction	Resin Content by Weight
269.80	52.09%	20.01%

Table 41. Pyrolysis Cycle for LBF107

PYROLYSIS CYCLE	
Ramp Up	1°C/min
Hold Temp	650°C
Hold Time	No Hold
Ramp Up	2°C/min
Hold Temp	850°C
Hold Time	90 minutes
Ramp Down	5°C/min

Table 42. Post Pyrolysis for LBF107

PYROLYSIS		
Initial Weight (g)	Post Weight (g)	Resin Retained (%)
279.30	260.00	69.61%

PANEL LBF203

Table 43. Materials for LBF203

MATERIALS					
Resin	Resin Weight (g)	Fiber	Layup	Fiber Weight (g)	Total Weight (g)
SMP-10	61.70	Biaxial Basalt Fiber	[0/90]11	201.70	263.40

Table 44. Cure Cycle for LBF203

CURE CYCLE	
Ramp Up	3°C/min
Hold Temp	170°C
Hold Time	90 min
Vacuum	-28 inHg
Pressure	20 psi
Post Cure Temp	275°C
Post Cure Hold	24 Hours

Table 45. Post Cure for LBF203

POST CURE		
Post Weight (g)	Fiber Volume Fraction	Resin Content by Weight
248.20	54.72%	18.73%

61

Table 46. Pyrolysis Cycle for LBF203

PYROLYSIS CYCLE	
Ramp Up	1°C/min
Hold Temp	650°C
Hold Time	No Hold
Ramp Up	2°C/min
Hold Temp	850°C
Hold Time	90 minutes
Ramp Down	5°C/min

Table 47. Post Pyrolysis for LBF203

PYROLYSIS		
Initial Weight (g)	Post Weight (g)	Resin Retained (%)
249.70	238.50	76.67%

PANEL LBF204

Table 48. Materials for LBF204

MATERIALS					
Resin	Resin Weight (g)	Fiber	Layup	Fiber Weight (g)	Total Weight (g)
SMP-10	80.00	Biaxial Basalt Fiber	[0/90]12	212.00	292.00

Table 49. Cure Cycle for LBF204

CURE CYCLE	
Ramp Up	3°C/min
Hold Temp	170°C
Hold Time	90 min
Vacuum	-28 inHg
Pressure	None
Post Cure Temp	275°C
Post Cure Hold	4 Hours

Table 50. Post Cure for LBF204

POST CURE		
Post Weight (g)	Fiber Volume Fraction	Resin Content by Weight
263.00	49.48%	19.39%

Table 51. Pyrolysis Cycle for LBF204

PYROLYSIS CYCLE	
Ramp Up	1°C/min
Hold Temp	200°C
Hold Time	60 min
Ramp Up	1°C/min
Hold Temp	400°C
Hold Time	60 min
Ramp Up	1°C/min
Hold Temp	600°C
Hold Time	60 min
Ramp Up	1°C/min
Hold Temp	700°C
Hold Time	60 min
Ramp Up	1°C/min
Hold Temp	850°C
Hold Time	60 min
Ramp Down	-0.75°C/min
Hold Temp	350°C
Hold Time	No Hold
Ramp Down	-1°C/min
Temp	100°C

Table 52. Post Pyrolysis for LBF204

PYROLYSIS		
Initial Weight (g)	Post Weight (g)	Resin Retained (%)
263.00	257.60	89.41%

PANEL LBF206

Table 53. Materials for LBF206

MATERIALS					
Resin	Resin Weight (g)	Fiber	Layup	Fiber Weight (g)	Total Weight (g)
SMP-10	81.60	Biaxial Basalt Fiber	[0/90]12	216.00	297.60

Table 54. Cure Cycle for LBF206

CURE CYCLE	
Ramp Up	3°C/min
Hold Temp	170°C
Hold Time	90 min
Vacuum	-28 inHg
Pressure	20 psi
Post Cure	275°C
Post Cure	24 Hours

Table 55. Post Cure for LBF206

POST CURE		
Post Weight (g)	Fiber Volume Fraction	Resin Content by Weight
273.00	49.45%	20.88%

Table 56. Pyrolysis Cycle for LBF206

PYROLYSIS CYCLE	
Ramp Up	1°C/min
Hold Temp	200°C
Hold Time	60 min
Ramp Up	1°C/min
Hold Temp	300°C
Hold Time	60 min
Ramp Up	1°C/min
Hold Temp	500°C
Hold Time	60 min
Ramp Up	1°C/min
Hold Temp	600°C
Hold Time	60 min
Ramp Up	1°C/min
Hold Temp	700°C
Hold Time	60 min
Ramp Up	1°C/min
Hold Temp	850°C
Hold Time	60 min
Ramp Down	-0.75°C/min
Temp	100°C

Table 57. Post Pyrolysis for LBF206

PYROLYSIS		
Initial Weight (g)	Post Weight (g)	Resin Retained (%)
276.00	268.00	86.67%

PANEL LBF207

Table 58. Materials for LBF207

MATERIALS					
Resin	Resin Weight (g)	Fiber	Layup	Fiber Weight (g)	Total Weight (g)
SMP-10	81.60	Biaxial Basalt Fiber	[0/90]12	218.00	299.60

Table 59. Cure Cycle for LBF207

CURE CYCLE	
Ramp Up	3°C/min
Hold Temp	170°C
Hold Time	90 min
Vacuum	-28 inHg
Pressure	20 psi

Table 60. Post Cure for LBF207

POST CURE		
Post Weight (g)	Fiber Volume Fraction	Resin Content by Weight
276.00	49.69%	21.01%

Table 61. Pyrolysis Cycle for LBF207

PYROLYSIS CYCLE	
Ramp Up	1.85°C/min
Hold Temp	260°C
Hold Time	180 min
Ramp Up	1°C/min
Hold Temp	300°C
Hold Time	60 min
Ramp Up	1°C/min
Hold Temp	500°C
Hold Time	60 min
Ramp Up	1°C/min
Hold Temp	600°C
Hold Time	60 min
Ramp Up	1°C/min
Hold Temp	700°C
Hold Time	60 min
Ramp Up	1°C/min
Hold Temp	850°C
Hold Time	60 min
Ramp Down	-0.75°C/min
Temp	100°C

PANEL LBF208

Table 62. Materials for LBF208

MATERIALS					
Resin	Resin Weight (g)	Fiber	Layup	Fiber Weight (g)	Total Weight (g)
SMP-10	81.60	Biaxial Basalt Fiber	[0/90]12	217.20	298.80

Table 63. Cure Cycle for LBF208

CURE CYCLE	
Ramp Up	3°C/min
Hold Temp	170°C
Hold Time	90 min
Vacuum	-28 inHg
Pressure	20 psi
Post Cure	275°C
Post Cure	24 Hours

Table 64. Post Cure for LBF208

POST CURE		
Post Weight (g)	Fiber Volume Fraction	Resin Content by Weight
270.60	49.59%	19.73%

Table 65. Pyrolysis Cycle for LBF208

PYROLYSIS CYCLE	
Ramp Up	1°C/min
Hold Temp	100°C
Hold Time	30 min
Ramp Up	1°C/min
Hold Temp	200°C
Hold Time	60 min
Ramp Up	1°C/min
Hold Temp	300°C
Hold Time	30 min
Ramp Up	1°C/min
Hold Temp	500°C
Hold Time	60 min
Ramp Up	1°C/min
Hold Temp	600°C
Hold Time	60 min
Ramp Up	1°C/min
Hold Temp	700°C
Hold Time	60 min
Ramp Up	1°C/min
Hold Temp	850°C
Hold Time	60 min
Ramp Down	-1°C/min
Temp	100°C

PANEL LBF214

Table 66. Materials for LBF214

MATERIALS					
Resin	Resin Weight (g)	Fiber	Layup	Fiber Weight (g)	Total Weight (g)
SMP-10	191.90	Biaxial Basalt Fiber	[0/90/45/-45/0/90/45/-45/0/90/45/-45]s	405.40	597.30

Table 67. Cure Cycle for LBF214

CURE CYCLE	
Ramp Up	3°C/min
Hold Temp	170°C
Hold Time	90 min
Vacuum	-28 inHg
Pressure	20 psi

Table 68. Post Cure for LBF214

PYROLYSIS		
Initial Weight (g)	Post Weight (g)	Resin Retained (%)
499.40	488.30	88.19%

Table 69. Pyrolysis Cycle for LBF214

PYROLYSIS CYCLE	
Ramp Up	1.85°C/min
Hold Temp	260°C
Hold Time	180 min
Ramp Up	1°C/min
Hold Temp	300°C
Hold Time	60 min
Ramp Up	1°C/min
Hold Temp	500°C
Hold Time	60 min
Ramp Up	1°C/min
Hold Temp	600°C
Hold Time	60 min
Ramp Up	1°C/min
Hold Temp	700°C
Hold Time	60 min
Ramp Up	1°C/min
Hold Temp	850°C
Hold Time	60 min
Ramp Down	-0.75°C/min
Temp	100°C

Table 70. Post Pyrolysis for LBF214

PYROLYSIS		
Initial Weight (g)	Post Weight (g)	Resin Retained (%)
499.40	488.30	88.19%

PANEL LBF215

Table 71. Materials for LBF215

MATERIALS					
Resin	Resin Weight (g)	Fiber	Layup	Fiber Weight (g)	Total Weight (g)
SMP-10	36.00	Plain Weave Basalt	[45/90/45/90]s	131.00	167.00

Table 72. Cure Cycle for LBF215

CURE CYCLE	
Ramp Up	3°C/min
Hold Temp	170°C
Hold Time	90 min
Vacuum	-28 inHg
Pressure	20 psi
Post Cure Temp	275°C
Post Cure Hold	18 Hours

Table 73. Post Cure for LBF215

POST CURE		
Post Weight (g)	Fiber Volume Fraction	Resin Content by Weight
154.30	57.36%	15.10%

Table 74. Pyrolysis Cycle for LBF215

PYROLYSIS CYCLE	
Ramp Up	1°C/min
Hold Temp	200°C
Hold Time	60 min
Ramp Up	1°C/min
Hold Temp	300°C
Hold Time	60 min
Ramp Up	1°C/min
Hold Temp	500°C
Hold Time	60 min
Ramp Up	1°C/min
Hold Temp	600°C
Hold Time	60 min
Ramp Up	1°C/min
Hold Temp	700°C
Hold Time	60 min
Ramp Up	1°C/min
Hold Temp	800°C
Hold Time	90 min
Ramp Down	-0.75°C/min
Temp	100°C

Table 75. Post Pyrolysis for LBF215

PYROLYSIS		
Initial Weight (g)	Post Weight (g)	Resin Retained (%)
158.60	157.60	96.38%

Table 76. Post Reinfiltration #1 for LBF215

REINFILTRATION AND PYROLYSIS CYCLE 1				
Initial Weight (g)	Post Reinfiltration Weight (g)	Post Pyrolysis Weight (g)	Resin Retained (%)	Resin Content by Weight
140.30	147.10	144.50	83.85%	19.29%

Table 77. Post Reinfiltration #2 for LBF215

REINFILTRATION AND PYROLYSIS CYCLE 2				
Initial Weight (g)	Post Reinfiltration Weight (g)	Post Pyrolysis Weight (g)	Resin Retained (%)	Resin Content by Weight
144.40	146.70	146.00	95.54%	20.12%

PANEL LBF216

Table 78. Materials for LBF216

MATERIALS					
Resin	Resin Weight (g)	Fiber	Layup	Fiber Weight (g)	Total Weight (g)
SMP-10	53.00	Plain Weave Basalt	[45/90/45/90/45/90]s	193.90	246.90

Table 79. Cure Cycle for LBF216

CURE CYCLE	
Ramp Up	3°C/min
Hold Temp	170°C
Hold Time	90 min
Ramp Down	3°C/min
Vacuum	28 inHg
Post Cure Temp	275°C
Post Cure Time	3 hours

Table 80. Post Cure for LBF216

POST CURE		
Weight (g)	Fiber Volume Fraction	Resin Content by Weight
236.80	57.49%	18.12%

Table 81. Pyrolysis Cycle for LBF216

PYROLYSIS CYCLE	
Ramp Up	1°C/min
Hold Temp	200°C
Hold Time	60 min
Ramp Up	1°C/min
Hold Temp	300°C
Hold Time	60 min
Ramp Up	1°C/min
Hold Temp	500°C
Hold Time	60 min
Ramp Up	1°C/min
Hold Temp	600°C
Hold Time	60 min
Ramp Up	1°C/min
Hold Temp	700°C
Hold Time	60 min
Ramp Up	1°C/min
Hold Temp	800°C
Hold Time	90 min
Ramp Down	-0.75°C/min

Table 82. Post Pyrolysis for LBF216

PYROLYSIS		
Initial Weight (g)	Post Weight (g)	Resin Retained (%)
236.80	230.00	84.15%

Table 83. Post Reinfiltration #1 for LBF216

REINFILTRATION AND PYROLYSIS CYCLE 1				
Initial Weight (g)	Post Reinfiltration Weight (g)	Post Pyrolysis Weight (g)	Resin Retained (%)	Resin Content by Weight
230.90	236.50	235.10	96.71%	17.52%

Table 84. Post Reinfiltration #2 for LBF216

REINFILTRATION AND PYROLYSIS CYCLE 2				
Initial Weight (g)	Post Reinfiltration Weight (g)	Post Pyrolysis Weight (g)	Resin Retained	Resin Content by Weight
234.90	238.40	237.00	96.85%	18.19%

PANEL LBF222

Table 85. Materials for LBF222

MATERIALS					
Resin	Resin Weight (g)	Fiber	Layup	Fiber Weight (g)	Total Weight (g)
SMP-10	47.00	Plain Weave Basalt	[90/90/90/90/45/45]s	161.00	208.00

Table 86. Cure Cycle for LBF222

CURE CYCLE	
Ramp Up	3°C/min
Hold Temp	170°C
Hold Time	90 min
Ramp Down	3°C/min
Vacuum	28 inHg

Table 87. Post Cure for LBF222

POST CURE		
Post Weight (g)	Fiber Volume Fraction	Resin Content by Weight
82.31%	55.87%	17.69%

Table 88. Pyrolysis Cycle for LBF222

PYROLYSIS CYCLE	
Ramp Up	1.8°C/min
Hold Temp	275°C
Hold Time	180 min
Ramp Up	1°C/min
Hold Temp	500°C
Hold Time	60 min
Ramp Up	1°C/min
Hold Temp	600°C
Hold Time	60 min
Ramp Up	1°C/min
Hold Temp	700°C
Hold Time	60 min
Ramp Up	1°C/min
Hold Temp	800°C
Hold Time	90 min
Ramp Down	-0.75°C/min

Table 89. Post Pyrolysis for LBF222

PYROLYSIS		
Initial Weight (g)	Post Weight (g)	Resin Retained
195.60	185.60	71.10%

Table 90. Reinfiltration Cycle for LBF222

PYROLYSIS CYCLE	
Ramp Up	1°C/min
Hold Temp	200°C
Hold Time	60 min
Ramp Up	1°C/min
Hold Temp	300°C
Hold Time	60 min
Ramp Up	1°C/min
Hold Temp	500°C
Hold Time	60 min
Ramp Up	1°C/min
Hold Temp	600°C
Hold Time	60 min
Ramp Up	1°C/min
Hold Temp	700°C
Hold Time	60 min
Ramp Up	1°C/min
Hold Temp	800°C
Hold Time	90 min
Ramp Down	-0.75°C/min

Table 91. Post Reinfiltration #1 for LBF222

REINFILTRATION AND PYROLYSIS CYCLE 1				
Initial Weight (g)	Post Reinfiltration Weight (g)	Post Pyrolysis Weight (g)	Resin Retained	Resin Content by Weight
185.60	210.60	198.80	76.21%	19.01%

Table 92. Post Reinfiltration #2 for LBF222

REINFILTRATION AND PYROLYSIS CYCLE 2				
Initial Weight (g)	Post Reinfiltration Weight (g)	Post Pyrolysis Weight (g)	Resin Retained	Resin Content by Weight
198.80	220.40	208.10	79.29%	22.63%

PANEL LBF224

Table 93. Materials for LBF224

MATERIALS					
Resin	Resin Weight (g)	Fiber	Layup	Fiber Weight (g)	Total Weight (g)
SMP-10	46.90	Plain Weave Basalt	[90/90/45/90/90/90]s	155.50	202.40

Table 94. Cure Cycle for LBF224

CURE CYCLE	
Ramp Up	3°C/min
Hold Temp	170°C
Hold Time	90 min
Ramp Down	3°C/min
Vacuum	28 inHg

Table 95. Post Cure for LBF224

POST CURE		
Post Weight (g)	Fiber Volume Fraction	Resin Content by Weight
190.90	55.07%	18.54%

Table 96. Pyrolysis Cycle for LBF224

PYROLYSIS CYCLE	
Ramp Up	1.8°C/min
Hold Temp	275°C
Hold Time	180 min
Ramp Up	1°C/min
Hold Temp	400°C
Hold Time	60 min
Ramp Up	1°C/min
Hold Temp	500°C
Hold Time	60 min
Ramp Up	1°C/min
Hold Temp	600°C
Hold Time	60 min
Ramp Up	1°C/min
Hold Temp	700°C
Hold Time	90 min
Ramp Down	-0.75°C/min

Table 97. Post Pyrolysis for LBF224

PYROLYSIS		
Initial Weight (g)	Post Weight (g)	Resin Retained
190.90	182.00	74.86%

Table 98. Reinfiltration Cycle for LBF224

PYROLYSIS CYCLE	
Ramp Up	1°C/min
Hold Temp	300°C
Hold Time	60 min
Ramp Up	1°C/min
Hold Temp	400°C
Hold Time	60 min
Ramp Up	1°C/min
Hold Temp	500°C
Hold Time	60 min
Ramp Up	1°C/min
Hold Temp	600°C
Hold Time	60 min
Ramp Up	1°C/min
Hold Temp	700°C
Hold Time	90 min
Ramp Down	-0.75°C/min

Table 99. Post Reinfiltration #1 for LBF224

REINFILTRATION AND PYROLYSIS CYCLE 1				
Initial Weight (g)	Post Reinfiltration Weight (g)	Post Pyrolysis Weight (g)	Resin Retained	Resin Content by Weight
181.40	207.00	192.60	72.04%	19.26%

Table 100. Post Reinfiltration #2 for LBF224

REINFILTRATION AND PYROLYSIS CYCLE 2				
Initial Weight (g)	Post Reinfiltration Weight (g)	Post Pyrolysis Weight (g)	Resin Retained	Resin Content by Weight
192.60	210.20	201.00	77.26%	22.64%

PANEL LBF225

Table 101. Materials for LBF225

MATERIALS					
Resin	Resin Weight (g)	Fiber	Layup	Fiber Weight (g)	Total Weight (g)
SMP-10	49.20	Plain Weave Basalt	[90/90/45/90/90/90]s	156.80	206.00

Table 102. Cure Cycle for LBF225

CURE CYCLE	
Ramp Up	3°C/min
Hold Temp	170°C
Hold Time	90 min
Ramp Down	3°C/min
Vacuum	28 inHg

Table 103. Post Cure for LBF225

POST CURE		
Post Weight (g)	Fiber Volume Fraction	Resin Content (%)
190.50	54.09%	17.69%

Table 104. Pyrolysis Cycle for LBF225

PYROLYSIS CYCLE	
Ramp Up	1.8°C/min
Hold Temp	275°C
Hold Time	180 min
Ramp Up	1°C/min
Hold Temp	400°C
Hold Time	60 min
Ramp Up	1°C/min
Hold Temp	500°C
Hold Time	60 min
Ramp Up	1°C/min
Hold Temp	600°C
Hold Time	60 min
Ramp Up	1°C/min
Hold Temp	700°C
Hold Time	90 min
Ramp Down	-0.75°C/min

Table 105. Post Pyrolysis for LBF225

PYROLYSIS		
Initial Weight (g)	Post Weight (g)	Resin Retained
190.50	181.50	73.29%

Table 106. Reinfiltration Cycle for LBF225

PYROLYSIS CYCLE	
Ramp Up	1°C/min
Hold Temp	300°C
Hold Time	60 min
Ramp Up	1°C/min
Hold Temp	400°C
Hold Time	60 min
Ramp Up	1°C/min
Hold Temp	500°C
Hold Time	60 min
Ramp Up	1°C/min
Hold Temp	600°C
Hold Time	60 min
Ramp Up	1°C/min
Hold Temp	700°C
Hold Time	90 min
Ramp Down	-0.75°C/min

Table 107. Post Reinfiltration #1 for LBF225

REINFILTRATION AND PYROLYSIS CYCLE 1				
Initial Weight (g)	Post Reinfiltration Weight (g)	Post Pyrolysis Weight (g)	Resin Retained	Resin Content by Weight
181.50	211.70	193.80	90.19%	19.09%

Table 108. Post Reinfiltration #2 for LBF225

REINFILTRATION AND PYROLYSIS CYCLE 2				
Initial Weight (g)	Post Reinfiltration Weight (g)	Post Pyrolysis Weight (g)	Resin Retained	Resin Content by Weight
193.80	215.30	202.00	77.26%	22.38%

APPENDIX B:COPYRIGHT LICENSE AGREEMENTS

SPRINGER LICENSE
TERMS AND CONDITIONS

Jun 30, 2014

This is a License Agreement between Sarah Cox ("You") and Springer ("Springer") provided by Copyright Clearance Center ("CCC"). The license consists of your order details, the terms and conditions provided by Springer, and the payment terms and conditions.

All payments must be made in full to CCC. For payment instructions, please see information listed at the bottom of this form.

License Number	3406300114118
License date	Jun 12, 2014
Licensed content publisher	Springer
Licensed content publication	Journal of Materials Science (full set)
Licensed content title	Composite polymer derived ceramic system for oxidizing environments
Licensed content author	Jessica D. Torrey
Licensed content date	Jan 1, 2006
Volume number	41
Issue number	14
Type of Use	Thesis/Dissertation
Portion	Figures
Author of this Springer article	No
Order reference number	None
Original figure numbers	Figure 1
Title of your thesis / dissertation	MATERIAL CHARACTERIZATION OF CONTINUOUS BASALT FIBER REINFORCED CERAMIC MATRIX COMPOSITES USING POLYMER DERIVED CERAMICS
Expected completion date	Jul 2014
Estimated size(pages)	50
Total	0.00 USD

Terms and Conditions

Introduction

The publisher for this copyrighted material is Springer Science + Business Media. By clicking "accept" in connection with completing this licensing transaction, you agree that the following terms and conditions apply to this transaction (along with the Billing and Payment terms and conditions established by Copyright Clearance Center, Inc. ("CCC"), at the time that you opened your Rightslink account and that are available at any time at http://myaccount.copyright.com).

Limited License

With reference to your request to reprint in your thesis material on which Springer Science and Business Media control the copyright, permission is granted, free of charge, for the use indicated in your enquiry.

Licenses are for one-time use only with a maximum distribution equal to the number that you identified in the licensing process.

This License includes use in an electronic form, provided its password protected or on the university's intranet or repository, including UMI (according to the definition at the Sherpa website: http://www.sherpa.ac.uk/romeo/). For any other electronic use, please contact Springer at (permissions.dordrecht@springer.com or permissions.heidelberg@springer.com).

The material can only be used for the purpose of defending your thesis limited to university-use only. If the thesis is going to be published, permission needs to be re-obtained (selecting "book/textbook" as the type of use).

Although Springer holds copyright to the material and is entitled to negotiate on rights, this license is only valid, subject to a courtesy information to the author (address is given with the article/chapter) and provided it concerns original material which does not carry references to other sources (if material in question appears with credit to another source, authorization from that source is required as well).

Permission free of charge on this occasion does not prejudice any rights we might have to charge for reproduction of our copyrighted material in the future.

Altering/Modifying Material: Not Permitted

You may not alter or modify the material in any manner. Abbreviations, additions, deletions and/or any other alterations shall be made only with prior written authorization of the author(s) and/or Springer Science + Business Media. (Please contact Springer at (permissions.dordrecht@springer.com or permissions.heidelberg@springer.com)

Reservation of Rights

Springer Science + Business Media reserves all rights not specifically granted in the combination of (i) the license details provided by you and accepted in the course of this licensing transaction, (ii) these terms and conditions and (iii) CCC's Billing and Payment terms and conditions.

Copyright Notice Disclaimer

You must include the following copyright and permission notice in connection with any reproduction of the licensed material: "Springer and the original publisher /journal title, volume, year of publication, page, chapter/article title, name(s) of author(s), figure number(s), original copyright notice) is given to the publication in which the material was originally published, by adding; with kind permission from Springer Science and Business Media"

Warranties: None

Example 1: Springer Science + Business Media makes no representations or warranties with

respect to the licensed material.

Example 2: Springer Science + Business Media makes no representations or warranties with respect to the licensed material and adopts on its own behalf the limitations and disclaimers established by CCC on its behalf in its Billing and Payment terms and conditions for this licensing transaction.

Indemnity
You hereby indemnify and agree to hold harmless Springer Science + Business Media and CCC, and their respective officers, directors, employees and agents, from and against any and all claims arising out of your use of the licensed material other than as specifically authorized pursuant to this license.

No Transfer of License
This license is personal to you and may not be sublicensed, assigned, or transferred by you to any other person without Springer Science + Business Media's written permission.

No Amendment Except in Writing
This license may not be amended except in a writing signed by both parties (or, in the case of Springer Science + Business Media, by CCC on Springer Science + Business Media's behalf).

Objection to Contrary Terms
Springer Science + Business Media hereby objects to any terms contained in any purchase order, acknowledgment, check endorsement or other writing prepared by you, which terms are inconsistent with these terms and conditions or CCC's Billing and Payment terms and conditions. These terms and conditions, together with CCC's Billing and Payment terms and conditions (which are incorporated herein), comprise the entire agreement between you and Springer Science + Business Media (and CCC) concerning this licensing transaction. In the event of any conflict between your obligations established by these terms and conditions and those established by CCC's Billing and Payment terms and conditions, these terms and conditions shall control.

Jurisdiction
All disputes that may arise in connection with this present License, or the breach thereof, shall be settled exclusively by arbitration, to be held in The Netherlands, in accordance with Dutch law, and to be conducted under the Rules of the 'Netherlands Arbitrage Instituut' (Netherlands Institute of Arbitration). *OR:*

All disputes that may arise in connection with this present License, or the breach thereof, shall be settled exclusively by arbitration, to be held in the Federal Republic of Germany, in accordance with German law.

Other terms and conditions:

v1.3

If you would like to pay for this license now, please remit this license along with your payment made payable to "COPYRIGHT CLEARANCE CENTER" otherwise you will be

invoiced within 48 hours of the license date. Payment should be in the form of a check or money order referencing your account number and this invoice number 501326217. Once you receive your invoice for this order, you may pay your invoice by credit card. Please follow instructions provided at that time.

Make Payment To:
Copyright Clearance Center
Dept 001
P.O. Box 843006
Boston, MA 02284-3006

For suggestions or comments regarding this order, contact RightsLink Customer Support: customercare@copyright.com or +1-877-622-5543 (toll free in the US) or +1-978-646-2777.

Gratis licenses (referencing $0 in the Total field) are free. Please retain this printable license for your reference. No payment is required.

SPRINGER LICENSE
TERMS AND CONDITIONS

Jun 30, 2014

This is a License Agreement between Sarah Cox ("You") and Springer ("Springer") provided by Copyright Clearance Center ("CCC"). The license consists of your order details, the terms and conditions provided by Springer, and the payment terms and conditions.

All payments must be made in full to CCC. For payment instructions, please see information listed at the bottom of this form.

License Number	3406300353326
License date	Jun 12, 2014
Licensed content publisher	Springer
Licensed content publication	Journal of Materials Science (full set)
Licensed content title	Conversion of polycarbosilane (PCS) to SiC-based ceramic Part 1. Characterisation of PCS and curing products
Licensed content author	H. Q. Ly
Licensed content date	Jan 1, 2001
Volume number	36
Issue number	16
Type of Use	Thesis/Dissertation
Portion	Figures
Author of this Springer article	No
Order reference number	None
Original figure numbers	Figure 6
Title of your thesis / dissertation	MATERIAL CHARACTERIZATION OF CONTINUOUS BASALT FIBER REINFORCED CERAMIC MATRIX COMPOSITES USING POLYMER DERIVED CERAMICS
Expected completion date	Jul 2014
Estimated size(pages)	50
Total	0.00 USD

Terms and Conditions

Introduction

The publisher for this copyrighted material is Springer Science + Business Media. By clicking "accept" in connection with completing this licensing transaction, you agree that the following terms and conditions apply to this transaction (along with the Billing and Payment terms and conditions established by Copyright Clearance Center, Inc. ("CCC"), at the time that you opened your Rightslink account and that are available at any time at http://myaccount.copyright.com).

Limited License

With reference to your request to reprint in your thesis material on which Springer Science and Business Media control the copyright, permission is granted, free of charge, for the use indicated in your enquiry.

Licenses are for one-time use only with a maximum distribution equal to the number that you identified in the licensing process.

This License includes use in an electronic form, provided its password protected or on the university's intranet or repository, including UMI (according to the definition at the Sherpa website: http://www.sherpa.ac.uk/romeo/). For any other electronic use, please contact Springer at (permissions.dordrecht@springer.com or permissions.heidelberg@springer.com).

The material can only be used for the purpose of defending your thesis limited to university-use only. If the thesis is going to be published, permission needs to be re-obtained (selecting "book/textbook" as the type of use).

Although Springer holds copyright to the material and is entitled to negotiate on rights, this license is only valid, subject to a courtesy information to the author (address is given with the article/chapter) and provided it concerns original material which does not carry references to other sources (if material in question appears with credit to another source, authorization from that source is required as well).

Permission free of charge on this occasion does not prejudice any rights we might have to charge for reproduction of our copyrighted material in the future.

Altering/Modifying Material: Not Permitted

You may not alter or modify the material in any manner. Abbreviations, additions, deletions and/or any other alterations shall be made only with prior written authorization of the author(s) and/or Springer Science + Business Media. (Please contact Springer at (permissions.dordrecht@springer.com or permissions.heidelberg@springer.com)

Reservation of Rights

Springer Science + Business Media reserves all rights not specifically granted in the combination of (i) the license details provided by you and accepted in the course of this licensing transaction, (ii) these terms and conditions and (iii) CCC's Billing and Payment terms and conditions.

Copyright Notice:Disclaimer

You must include the following copyright and permission notice in connection with any reproduction of the licensed material: "Springer and the original publisher /journal title, volume, year of publication, page, chapter/article title, name(s) of author(s), figure number(s), original copyright notice) is given to the publication in which the material was originally published, by adding; with kind permission from Springer Science and Business Media"

Warranties: None

Example 1: Springer Science + Business Media makes no representations or warranties with

95

respect to the licensed material.

Example 2: Springer Science + Business Media makes no representations or warranties with respect to the licensed material and adopts on its own behalf the limitations and disclaimers established by CCC on its behalf in its Billing and Payment terms and conditions for this licensing transaction.

Indemnity
You hereby indemnify and agree to hold harmless Springer Science + Business Media and CCC, and their respective officers, directors, employees and agents, from and against any and all claims arising out of your use of the licensed material other than as specifically authorized pursuant to this license.

No Transfer of License
This license is personal to you and may not be sublicensed, assigned, or transferred by you to any other person without Springer Science + Business Media's written permission.

No Amendment Except in Writing
This license may not be amended except in a writing signed by both parties (or, in the case of Springer Science + Business Media, by CCC on Springer Science + Business Media's behalf).

Objection to Contrary Terms
Springer Science + Business Media hereby objects to any terms contained in any purchase order, acknowledgment, check endorsement or other writing prepared by you, which terms are inconsistent with these terms and conditions or CCC's Billing and Payment terms and conditions. These terms and conditions, together with CCC's Billing and Payment terms and conditions (which are incorporated herein), comprise the entire agreement between you and Springer Science + Business Media (and CCC) concerning this licensing transaction. In the event of any conflict between your obligations established by these terms and conditions and those established by CCC's Billing and Payment terms and conditions, these terms and conditions shall control.

Jurisdiction
All disputes that may arise in connection with this present License, or the breach thereof, shall be settled exclusively by arbitration, to be held in The Netherlands, in accordance with Dutch law, and to be conducted under the Rules of the 'Netherlands Arbitrage Instituut' (Netherlands Institute of Arbitration). *OR:*

All disputes that may arise in connection with this present License, or the breach thereof, shall be settled exclusively by arbitration, to be held in the Federal Republic of Germany, in accordance with German law.

Other terms and conditions:

v1.3

If you would like to pay for this license now, please remit this license along with your payment made payable to "COPYRIGHT CLEARANCE CENTER" otherwise you will be

invoiced within 48 hours of the license date. Payment should be in the form of a check or money order referencing your account number and this invoice number 501326222. Once you receive your invoice for this order, you may pay your invoice by credit card. Please follow instructions provided at that time.

Make Payment To:
Copyright Clearance Center
Dept 001
P.O. Box 843006
Boston, MA 02284-3006

For suggestions or comments regarding this order, contact RightsLink Customer Support: customercare@copyright.com or +1-877-622-5543 (toll free in the US) or +1-978-646-2777.

Gratis licenses (referencing $0 in the Total field) are free. Please retain this printable license for your reference. No payment is required.

REFERENCES

1. Calle, L., Hintze, P., Parlier, C., Sampson, J., Curran, J., Kolody, M., & Perusich, S. (2010). Refractory materials for flame deflector protection. *AIAA SPACE 2010 Conference and Exposition,*

2. Cerny, M., Glogar, P., Golias, V., Hruska, J., Jakes, P., Sucharda, Z., & Vavrova, I. (2007). Comparison of mechanical properties and structural changes of continuous basalt and glass fibres at elevated temperatures. *CERAMICS-SILIKATY, 51*(2), 82-88. Retrieved from http://ezproxy.net.ucf.edu/login?url=http://search.ebscohost.com/login.aspx?direct=true&db=edswsc&AN=000249498400003&site=eds-live&scope=site

3. Cerny, M., Halasova, M., Schwaigstillova, J., Chlup, Z., Sucharda, Z., Glogar, P., . . . Ryglova, S. (2014). Mechanical properties of partially pyrolysed composites with plain weave basalt fibre reinforcement. *Ceramics International, 40*(5), 7507-7521. Retrieved from http://ezproxy.net.ucf.edu/login?url=http://search.ebscohost.com/login.aspx?direct=true&db=edswsc&AN=000333488100141&site=eds-live&scope=site

4. Czigány, T. (2005). Discontinuous basalt fiber-reinforced hybrid composites. *Polymer Composites (9780387241760),* , 309. Retrieved from http://ezproxy.net.ucf.edu/login?url=http://search.ebscohost.com/login.aspx?direct=true&db=edb&AN=76801963&site=eds-live&scope=site

5. Glogar, P., Sucharda, Z., Cerny, M., Puchegger, S., & Peterlik, H. (2007). Microstructure and mechanical properties of heat resistant composites reinforced with basalt fibres. *CERAMICS-SILIKATY, 51*(4), 190-197. Retrieved from

http://ezproxy.net.ucf.edu/login?url=http://search.ebscohost.com/login.aspx?direct=true&db=edswsc&AN=000252181900002&site=eds-live&scope=site

6. Gumula, T., & Blazewicz, S. (2013). Thermal conversion of carbon fibres/polysiloxane composites to carbon fibres/ceramic composites. *Ceramics International, 39*(4), 3795-3802. doi:http://dx.doi.org/10.1016/j.ceramint.2012.10.219

7. Gumula, T., Paluszkiewicz, C., & Blazewicz, S. (2009). Study on thermal decomposition processes of polysiloxane polymers—From polymer to nanosized silicon carbide. *Journal of Analytical and Applied Pyrolysis, 86*(2), 375-380. doi:http://dx.doi.org.ezproxy.net.ucf.edu/10.1016/j.jaap.2009.09.001

8. Hague, M. H., Upadhyaya, P., Roy, S., Ware, T., Voit, W., & Lu, H. B. (2014). *The changes in flexural properties and microstructures of carbon fiber bismaleimide composite after exposure to a high temperature* Retrieved from http://ezproxy.net.ucf.edu/login?url=http://search.ebscohost.com/login.aspx?direct=true&db=edswsc&AN=000329881500007&site=eds-live&scope=site

9. Ivanitskii, S. G., & Gorbachev, G. F. (2011). Continuous basalt fibers: Production aspects and simulation of forming processes. I. state of the art in continuous basalt fiber technologies. *POWDER METALLURGY AND METAL CERAMICS, 50*(3-4), 125-129. Retrieved from http://ezproxy.net.ucf.edu/login?url=http://search.ebscohost.com/login.aspx?direct=true&db=edswsc&AN=000293469700001&site=eds-live&scope=site

10. Landucci, G., Rossi, F., Nicolella, C., & Zanelli, S. (2009). Design and testing of innovative materials for passive fire protection. *Fire Safety Journal,* (8), 1103. doi:10.1016/j.firesaf.2009.08.004

11. Ly, H. Q., Taylor, R., & Day, R. J. (2001a). Conversion of polycarbosilane (PCS) to SiC-based ceramic. part 1. characterisation of PCS and curing products. *Journal of Materials Science, 36*(16), 4037-4043. Retrieved from

http://ezproxy.net.ucf.edu/login?url=http://search.ebscohost.com/login.aspx?direct=true&db=asf&AN=500789299&site=eds-live&scope=site

12. Ly, H. Q., Taylor, R., & Day, R. J. (2001b). Conversion of polycarbosilane (PCS) to SiC-based ceramic. part II. pyrolysis and characterisation. *Journal of Materials Science, 36*(16), 4045-4057. Retrieved from

http://ezproxy.net.ucf.edu/login?url=http://search.ebscohost.com/login.aspx?direct=true&db=asf&AN=500789292&site=eds-live&scope=site

13. Ma, Y., & Chen, Z. H. (2013). Microstructures and properties of the C/zr-O-si-C composites fabricated by polymer infiltration and pyrolysis. *JOURNAL OF MATERIALS ENGINEERING AND PERFORMANCE, 22*(9), 2510-2514. Retrieved from

http://ezproxy.net.ucf.edu/login?url=http://search.ebscohost.com/login.aspx?direct=true&db=edswsc&AN=000323425100010&site=eds-live&scope=site

14. Mangalgiri, P. (2005). Polymer-matrix composites for high-temperature applications. *Defence Science Journal, 55*(2) Retrieved from

http://publications.drdo.gov.in/ojs/index.php/dsj/article/view/1980

15. Militky, J., & Kovacic, V. (2000). Ultimate mechanical properties of thermally exposed basalt filament yarns. *MOLECULAR CRYSTALS AND LIQUID CRYSTALS, 354*, 643-650. Retrieved from

http://ezproxy.net.ucf.edu/login?url=http://search.ebscohost.com/login.aspx?direct=true&db=edswsc&AN=000168131800007&site=eds-live&scope=site

16. Naslain, R. (1999). Materials design and processing of high temperature ceramic matrix composites: State of the art and future trends. *ADVANCED COMPOSITE MATERIALS, 8*(1), 3-16. Retrieved from

http://ezproxy.net.ucf.edu/login?url=http://search.ebscohost.com/login.aspx?direct=true&db=edswsc&AN=000079219400002&site=eds-live&scope=site

17. Nicholas, J. L., Menta, V. G. A., Chandrashekhara, K., Watts, J., Lai, B., Hilmas, G., & Fahrenholtz, W. (2012). Processing of continuous fiber reinforced ceramic composites for ultra high termperature applications using polymer precursors. *Society for the Advancement of Materials Ad Process Engineering,* Baltimore, MD.

18. Novitskii, A., & Efremov, M. (2011). Some aspects of the manufacturing process for obtaining continuous basalt fiber. *Glass & Ceramics, 67*(11), 361-365. doi:10.1007/s10717-011-9299-7

19. Novitskii, A. G., & Efremov, M. V. (2013). Technological aspects of the suitability of rocks from different deposits for the production of continuous basalt fiber. *GLASS AND CERAMICS, 69*(11-12), 409-412. Retrieved from

http://ezproxy.net.ucf.edu/login?url=http://search.ebscohost.com/login.aspx?direct=true&db=edswsc&AN=000316764200013&site=eds-live&scope=site

20. Project morpheus. Retrieved, 2013, Retrieved from http://morpheuslander.jsc.nasa.gov/about/

21. *Refractory concrete, specification for* (1979). NASA.

22. Singha, K. (2012). A short review on basalt fiber. *International Journal of Textile Science, 1*(4), 19.

23. SWORDS: Soldier-warfighter operationally responsive deployer for space. Retrieved, 2013, Retrieved from http://www.smdc.army.mil/FactSheets/SWORDS.pdf

24. System failure case studies: Hit the bricks. (2010). Retrieved, 2013, Retrieved from http://nsc.nasa.gov/SFCS/Index/SortByDate/Descending/Page3

25. Torrey, J. D., Bordia, R. K., Henager, J.,Charles H., Blum, Y., Shin, Y., & Samuels, W. D. (2006). Composite polymer derived ceramic system for oxidizing environments. *Journal of Materials Science, 41*(14), 4617-4622. doi:10.1007/s10853-006-0242-1

26. von Eckroth, W., Struchen, L., Trovillion, T., Perez, R., Nerolich, S., & Parlier, C. (2012). Space shuttle solid rocket motor plume pressure and heat rate measurements. *28th Aerodynamic Measurement Technology, Ground Testing, and Flight Testing Conference,* New Orleans, LA. doi:10.2514/6.2012-3293

27. YAJIMA, S., SHISHIDO, T., KAYANO, H., OKAMURA, K., OMORI, M., & HAYASHI, J. (1976). SiC sintered bodies with three-dimensional polycarbosilane as binder. *Nature, 264*(5583), 238. Retrieved from http://ezproxy.net.ucf.edu/login?url=http://search.ebscohost.com/login.aspx?direct=true&db=edb&AN=61731814&site=eds-live&scope=site

28. Ying, S., & Zhou, X. (2013). Chemical and thermal resistance of basalt fiber in inclement environments. *Journal of Wuhan University of Technology (Material Science Edition),* (3), 560. Retrieved from

http://ezproxy.net.ucf.edu/login?url=http://search.ebscohost.com/login.aspx?direct=true&db
=edsgao&AN=edsgcl.331993671&site=eds-live&scope=site

29. Zheng, G. B., Sano, H., Suzuki, K., Kobayashi, K., Uchiyama, Y., & Cheng, H. M. (1999). A

    TEM study of microstructure of carbon fiber/polycarbosilane-derived SiC composites.

    CARBON, 37(12), 2057-2062. Retrieved from

    http://ezproxy.net.ucf.edu/login?url=http://search.ebscohost.com/login.aspx?direct=true&db
    =edswsc&AN=000083985000022&site=eds-live&scope=site